universität wien

MASTERARBEIT | MASTER'S THESIS

Titel | Title

Phase stabilization for long fiber interferometry

verfasst von | submitted by

Lukas Steinbach BSc

angestrebter akademischer Grad | in partial fulfilment of the requirements for the degree of

Master of Science (MSc)

Wien | Vienna, 2025

Studienkennzahl lt. Studienblatt | Degree programme code as it appears on the student record sheet:	UA 066 876
Studienrichtung lt. Studienblatt | Degree programme as it appears on the student record sheet:	Masterstudium Physics
Betreut von | Supervisor:	Univ.-Prof. Dipl.-Ing. Dr. Philip Walther

Abstract

In physics, two fundamental theories describe the laws of nature: quantum mechanics and general relativity. Quantum mechanics governs the behavior of particles at the microscopic scale, such as photons and electrons, while general relativity describes the dynamics of massive objects on a macroscopic scale, including planets and galaxies. Both theories have been extensively tested and provide remarkably accurate descriptions of physical phenomena within their respective domains. However, a major challenge in modern physics arises when attempting to reconcile these two frameworks into a unified theory.

The objective of this master thesis is to take a contribution to the already existing gravites project [5], by designing an experimental setup to investigate gravitational effects on quantum systems. The proposed experiment involves constructing a Mach-Zehnder interferometer with arms positioned at different heights. Due to the height difference, the interferometer arms experience distinct gravitational potentials, leading to a gravitationally induced phase shift that increases with arm length. A key question this experiment seeks to address is whether quantum particles in a superposition state, propagating through the interferometer, experience distinct gravitational fields in comparison to classical predictions. To realize this experiment, several technical challenges must be overcome. One crucial aspect is stabilizing the interferometric phase as the arm length increases, given that background noise also increases with longer paths. Identifying and mitigating these noise sources is essential for extending the system operational limits and laying the groundwork for future research.

The initial phase of the project involves constructing a simple fiber-based Mach-Zehnder interferometer and characterizing key parameters such as visibility. Step-by-step refinements lead to a setup incorporating a fiber stretcher and a feedback control system designed to stabilize the phase. However, as the arm length is extended, maintaining phase stability becomes increasingly difficult, with the systems limitations becoming apparent at an arm length of 15 meters, far shorter than the required scale for meaningful gravitational effects. To address this limitation, a second setup is theoretically developed, replacing the fiber stretcher with two acousto-optic modulator (AOM) and implementing an improved feedback loop. This modification enables enhanced phase control over longer arm lengths. Ultimately, this thesis establishes a foundation for further experimental advancements within the research group, paving the way for future investigations into the interplay between quantum mechanics and general relativity.

Zusammenfassung

In der Physik beschreiben zwei fundamentale Theorien die Gesetze der Natur: die Quantenmechanik und die allgemeine Relativitätstheorie. Während die Quantenmechanik das Verhalten von Teilchen auf mikroskopischer Skala, wie Photonen und Elektronen, beschreibt, erfasst die allgemeine Relativitätstheorie die Dynamik massereicher Objekte auf makroskopischer Skala. Beide Theorien wurden umfassend experimentell überprüft und liefern äußerst präzise Beschreibungen physikalischer Phänomene innerhalb ihrer jeweiligen Gültigkeitsbereiche. Eine zentrale Herausforderung der modernen Physik besteht jedoch darin, diese beiden theoretischen Rahmenwerke in einer einheitlichen Theorie zu vereinen.

Diese Masterarbeit leistet einen Beitrag zum GRAVITES-Projekt [5], indem ein experimenteller Aufbau entwickelt wird, der gravitative Effekte auf Quantensysteme untersucht. Das geplante Experiment basiert auf einem Mach-Zehnder-Interferometer mit Armen auf unterschiedlichen Höhen. Dadurch erfahren die Arme unterschiedliche Gravitationspotenziale, was zu einer Gravitations bedingten Phasenverschiebung führt. Eine zentrale Fragestellung ist, ob Quantenpartikel in einem Superpositionszustand, die sich durch das Interferometer bewegen, unterschiedliche Gravitationsfelder erfahren im Vergleich zur klassischen Physik. Ein wesentlicher Aspekt des Experiments ist die Stabilisierung der Phase, da längere Lichtwege anfälliger für Hintergrundrauschen sind.

In der ersten Phase wird ein einfaches Mach-Zehnder-Interferometer aufgebaut und charakterisiert. Durch schrittweise Optimierung wird ein System mit einem Faserstrecker und einem Rückkopplungssystem entwickelt. Allerdings wird mit zunehmender Armlänge die Phasenkontrolle zunehmend schwieriger, sodass die experimentellen Grenzen des Systems bei einer Armlänge von 15 Metern erreicht werden, eine Distanz, die für signifikante gravitative Effekte nicht ausreicht. Um diese Einschränkung zu überwinden, wird ein alternatives Setup entwickelt, das den Faserstrecker durch zwei akustische-optische Modulatoren (AOM) ersetzt. Diese Modifikationen ermöglichen eine präzisere Phasenkontrolle über größere Armlängen. Letztlich legt diese Arbeit die experimentellen Grundlagen für zukünftige Weiterentwicklungen innerhalb der Arbeitsgruppe und weiterführende Untersuchungen zum Zusammenspiel von Quantenmechanik und allgemeiner Relativitätstheorie.

Acknowledgements

First and foremost, I would like to express my sincere gratitude to my supervisor, Univ.-Prof. Dipl.-Ing. Dr. Philip Walther, for giving me the opportunity to work in his group. From the very first day, I was deeply interested in the project, and I am truly proud to have been a part of it. I would also like to thank all the members of the gravity group with whom I had the privilege to work. The working environment was always both, intellectually stimulating and respectful. In particular, I want to express my appreciation to PhD R.W. Peterson, whose guidance was invaluable at the beginning of my thesis. His support not only helped me gain a solid start in the project but also allowed me to find my place within the group. Furthermore, I extend my sincere thanks to PhD H. Yu for the excellent collaboration during the second phase of my thesis. Thank you for the many hours we spent together in the lab and for all the knowledge I was able to gain from you.

Special thanks go to all my friends from the faculty of physics. It has always been a pleasure to work in such an inspiring environment, surrounded by friends I could always rely on. Here, I would like to mention two individuals in particular: Felix Hitzelhammer and Harald Kail. I am deeply grateful for the incredible time we shared, for the countless hours of laughter in the lab, but also for the days when things were more challenging. Your unwavering support throughout the past years has meant a lot to me and the time with you is filled with invaluable memories.

Finally, I would like to express my deepest gratitude to my family, especially my parents, Sabine Steinbach and Erwin Steinbach. None of this would have been possible without you. Thank you for giving me the opportunity to pursue my passion and build a career in physics. Your unconditional support throughout my life has been the foundation of my journey, and for that, I am eternally grateful.

Contents

1 Introduction **9**

1.1 Bridging quantum mechanics and general relativity 9
1.2 Idea of the experiment 11
1.3 Goal of the master thesis 13

2 Theoretical Background **14**

2.1 Shapiro delay 14
2.2 Quantum superposition 15
2.3 Setup of the experiment 17
2.3.1 Mach-Zehnder interferometer 18
2.3.2 Components of fiber interferometry 21
2.3.3 Phase shift $\Delta\phi$ 23
2.3.4 Polarization 25
2.4 Noise sources in the system 28
2.4.1 Laser phase noise 28
2.4.2 Fiber thermal noise 29
2.4.3 Other noise sources and system limitations 29
2.5 Feedback-Loop 30
2.5.1 Positive feedback 30
2.5.2 Negative feedback 31

3 Experimental setup: MZI with analog feedback loop and fiber stretcher **33**

3.1 First setup: Simple Mach-Zehnder 33
3.1.1 Experimental setup 35
3.1.2 Measurement 37
3.2 Second setup: Fiber stretcher + analog feedback loop 41
3.2.1 Experimental setup 42
3.2.2 Measurement 45
3.3 Third setup: Limit of the feedback board 47
3.3.1 5 m fiber 47
3.3.2 15 m fiber 49
3.3.3 1 km fiber spool 50
3.3.4 Shielding techniques and environmental factors 51
3.4 Conclusion so far 51

4 Improved setup: MZI with two AOM and PLL **52**

4.1 Review 52
4.2 AOM and PLL 54

4.3 Implemantation and calculation 57

5 Conclusion **63**

6 Bibliography **64**

6.1 List of references 64

6.2 List of components 66

1 Introduction

1.1 Bridging quantum mechanics and general relativity

In modern physics, two fundamental frameworks govern our understanding of nature: quantum mechanics and general relativity. While each theory has been remarkably successful within its respective domain, significant challenges arise when attempting to reconcile them into a single, unified framework [1]. Consequently, a major objective in contemporary theoretical physics is to establish a consistent theory that seamlessly integrates both quantum mechanics and general relativity, often referred to as the "theory of everything." Such a theory would provide a comprehensive description of the fundamental forces and interactions in the universe, resolving the inconsistencies that emerge at the interface of these two paradigms.

Each of these theories excels in describing physical phenomena within its designated scale. General relativity, formulated by Albert Einstein [2], provides an exceptionally accurate description of gravity on macroscopic scales, from planetary motion to the dynamics of entire galaxies and even the large-scale structure of the universe. Over the past century, numerous experimental and observational confirmations, ranging from gravitational lensing to the detection of gravitational waves, have validated Einsteins predictions, further solidifying our understanding of spacetime curvature and gravitational interactions.

However, when transitioning to microscopic scales, such as atomic and subatomic levels, the classical framework of general relativity becomes inadequate. Instead, quantum mechanics governs the behavior of fundamental particles and interactions at these scales. The quantum world is inherently probabilistic, contrasting sharply with the deterministic nature of general relativity. Notions such as wave-particle duality, superposition, and quantum entanglement introduce a paradigm that seems disconnected from the smooth, continuous fabric of spacetime described by general relativity. Furthermore, the conventional understanding of space and time itself becomes ambiguous at quantum scales, where quantum fluctuations lead to a breakdown of classical concepts.

Given these profound disparities, numerous theoretical and experimental efforts aim to bridge the gap between these two pillars of physics. Broadly speaking, two major research directions are pursued. One approach involves testing gravitational effects at increasingly smaller scales, probing the limits at which general relativity ceases to be valid and quantum effects begin to dominate. The complementary approach seeks to extend quantum mechanical principles to increasingly larger systems, exploring whether quantum behavior persists at macroscopic scales or whether a transition to classical behavior occurs under specific conditions.

Significant progress has already been made in this pursuit, yet a fully developed "theory of everything" remains elusive. The University of Vienna has played a pivotal role in advancing research in quantum mechanics, contributing to the broader effort of unifying these two theoretical frameworks. In particular, the groundbreaking work of Anton Zeilinger [3], who was awarded the Nobel Prize in Physics in 2022 for his contributions to quantum physics, has been instrumental in furthering our understanding of fundamental quantum principles. One of his major contributions includes experimental demonstrations of the violation of the Bell inequalities, confirming the existence of quantum entanglement and the apparent possibility of information transfer at speeds exceeding the speed of light. This phenomenon challenges the constraints imposed by relativity, highlighting the need for a more comprehensive theory that reconciles these conflicting aspects of modern physics.

This master thesis aims to contribute to the research group of Prof. Walther, laying the groundwork for future projects in the ongoing effort to connect quantum mechanics and general relativity.

1.2 Idea of the experiment

The central idea of this experiment is to construct a fiber-based Mach-Zehnder interferometer (MZI) in which the two arms are positioned at different heights, as illustrated in Fig. 1. Due to this vertical displacement, the arms experience slightly different gravitational potentials, leading to a phase shift induced by the gravitational time delay, commonly referred to as the Shapiro delay.

In general relativity, the Shapiro effect describes the additional time delay experienced by light or other particles as they travel through a gravitational field. This effect arises due to the warping of spacetime caused by massive bodies, altering the effective optical path length. When applied to an interferometric setup, this gravitationally induced delay manifests as a phase difference between the two paths, which can be observed in the interference pattern at the output of the interferometer.

A fundamental question that arises in this context is whether quantum particles in a superposition state, propagating through the interferometer, experience distinct gravitational interactions. Specifically, does the presence of superposition alter the gravitational phase shift in a way that deviates from classical predictions? This question lies at the heart of ongoing efforts to probe the interplay between quantum mechanics and general relativity. If measurable deviations from classical expectations are observed, they could provide valuable insights into the nature of gravity at quantum scales and contribute to the search for a unified theory.

This experiment aims to explore such quantum-gravitational effects by leveraging high-precision interferometry. By analyzing the phase shift induced by the Shapiro delay in a quantum superposition state, one can investigate whether quantum particles exhibit a novel response to gravitational fields, offering potential evidence for or against alternative formulations of quantum gravity.

This theoretical phase shift can be calculated via [4]:

$$\Delta\phi_g = \frac{2\pi Ang}{\lambda c^2} \tag{1}$$

n ... group index of refraction
λ ... center wavelength of the light
c ... speed of light in vacuum
g ... gravitational acceleration
A=l*h ... projected vertical enclosed area of the MZI

With the appropriate set of parameters, such a measurement could, in principle, be conducted on a laboratory scale, providing a feasible experimental setup for investigating gravitationally induced phase shifts in an interferometric system.: [4]

l=100 km, realized by spools
n=1,46 in each arm
h=2 m as height difference
λ= 1550 nm, wavelength of the laser

This should produce a phase shift of $\Delta\phi_g \approx 10^{-4}$ rad compared to the case with none height difference.

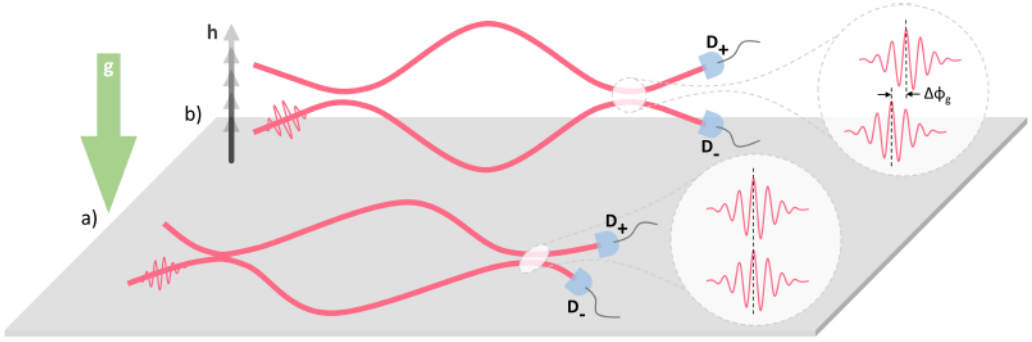

Figure 1: Illustration of the proposed experiment.
(Source:[4])

1.3 Goal of the master thesis

The primary objective of this master thesis is to contribute to the ongoing GRAVITES project [5] at the University of Vienna. The GRAVITES project is dedicated to conducting experiments at the interface between quantum mechanics and general relativity, aiming to explore the gravitational properties of single and entangled photons within the framework of Einsteins gravity. Such an experiment seeks to directly investigate how individual quantum particles respond to gravitational effects, addressing fundamental questions in the search for a unified physical theory.

The core of this thesis is to construct and optimize a fiber interferometric setup, as illustrated in Fig. 1.
The experimental approach is structured in a stepwise manner. The first stage involves assembling a basic fiber Mach-Zehnder interferometer (MZI) and characterizing its fundamental properties, including stability, phase coherence, and loss mechanisms. Once the primary characteristics are understood, the next phase will focus on pushing the system to its operational limits. Due to the extended arm length required for the experiment, significant noise sources, such as thermal fluctuations, mechanical vibrations, and environmental perturbations are expected to impact the interferometric measurements. A key aspect of this thesis will be to identify, quantify, and mitigate these noise contributions to enhance the stability and sensitivity of the setup.
Further improvements will be made iteratively, with the goal of increasing the effective arm length while maintaining phase coherence. The ultimate aim is to establish an experimental foundation that enables future investigations into gravitational effects on quantum states.
This work represents a crucial step toward the broader objectives of GRAVITES, advancing the frontier of quantum experiments in gravitational fields and potentially offering novel insights into the interplay between quantum mechanics and general relativity.

2 Theoretical Background

Before discussing the details of the experimental setup, it is essential to provide a theoretical foundation for the key concepts underlying this work. One of the fundamental effects relevant to this study is the Shapiro delay, which arises from general relativity and plays a crucial role in understanding how gravitational fields influence the propagation of light and matter waves.

2.1 Shapiro delay

The Shapiro delay [6] is a well-established effect predicted by general relativity. It is one of the key experimental confirmations of Einsteins theory and has been verified through numerous high-precision observations. This effect describes the additional time delay experienced by light as it propagates through a gravitational field, particularly when passing near a massive object (see Fig. 2).

In the framework of general relativity, massive objects cause a curvature of spacetime, affecting the trajectories of particles and electromagnetic waves. As a consequence, light traveling in the vicinity of a massive body follows a curved geodesic rather than a straight-line path in flat spacetime. This curvature results in an increase in the effective optical path length, leading to a measurable time delay compared to the case where no gravitational influence is present. Importantly, this effect is not exclusive to light but applies to any form of matter or radiation moving through a gravitational potential.

A particularly intriguing question arises when considering the Shapiro delay in the context of quantum superposition. In quantum mechanics, particles in a superposition state do not possess a well-defined position in space and time. This leads to the fundamental question: Do quantum particles in superposition experience the same gravitational time delay as classical objects? Since their spatial position is inherently uncertain, it remains unclear how gravitational effects, such as the Shapiro delay, manifest at the quantum level. Addressing this question requires a deeper examination of the principles of quantum superposition, which will be discussed in the following section.

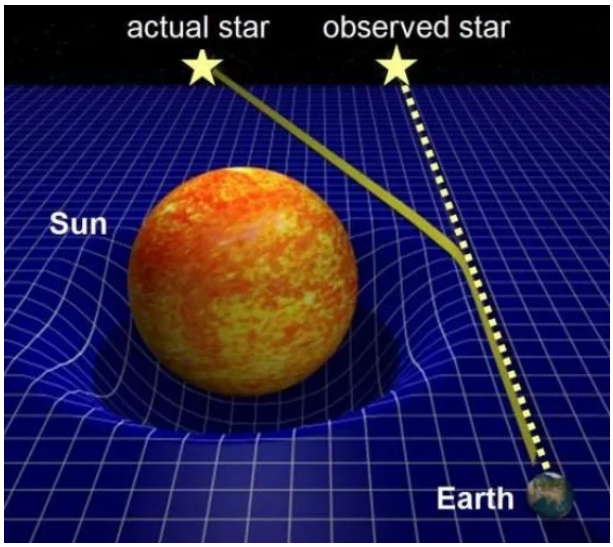

Figure 2: Shapiro delay
(Source: https://de.slideshare.net/slideshow/space-and-time-55946518/55946518)

2.2 Quantum superposition

One of the most fundamental and well-known experiments in quantum mechanics is the double-slit experiment [7]. This experiment provides profound insights into the wave-particle duality of quantum objects and remains one of the most striking demonstrations of quantum superposition.

In the classical setup, a beam of particles, such as electrons, is directed toward a barrier containing two narrow slits (see Fig. 3). Some of the electrons pass through one of the slits and subsequently strike a detection screen placed behind the barrier, while others are scattered in different directions. A classical intuition would suggest that the electrons, behaving as discrete particles, should produce two distinct bands on the screen, corresponding to the two slits. However, experimental observations reveal a strikingly different outcome: instead of two separate bands, an interference pattern emerges, characteristic of wave-like behavior. This result implies that each individual electron exhibits self-interference, as if it simultaneously traverses both slits.

An even more intriguing aspect of this phenomenon arises when one attempts to determine the precise path of the electrons by placing a measuring device (e.g., a detector or camera) at the slits. As soon as the path information is obtained, the interference pattern disappears, and the electrons behave like classical particles, forming two distinct bands on the detection screen. This phenomenon, known as "quantum superposition", suggests that an electron can exist in multiple states (i.e., passing through both slits) until a measurement forces it into a definite state.

This peculiar behavior remains one of the greatest mysteries in quantum mechanics. The underlying principle, often referred to as wave-particle duality, states that quantum entities such as electrons, neutrons, and protons exhibit both particle-like and wave-like properties depending on the experimental conditions. This duality has been confirmed not only for fundamental particles but also for larger molecular structures such as fullerenes, demonstrating that quantum effects persist at mesoscopic scales.

A key question that arises from this experiment in the context of this thesis is: How does a quantum particle in superposition respond to a gravitational field? If the particle is placed in a double-slit setup near a massive object, gravitational effects could influence its trajectory. Since the particle's exact position (i.e., which slit it passes through) remains undefined until measured, it is unclear how gravity acts upon it. Investigating this question could provide new insights into the interaction between quantum mechanics and general relativity.

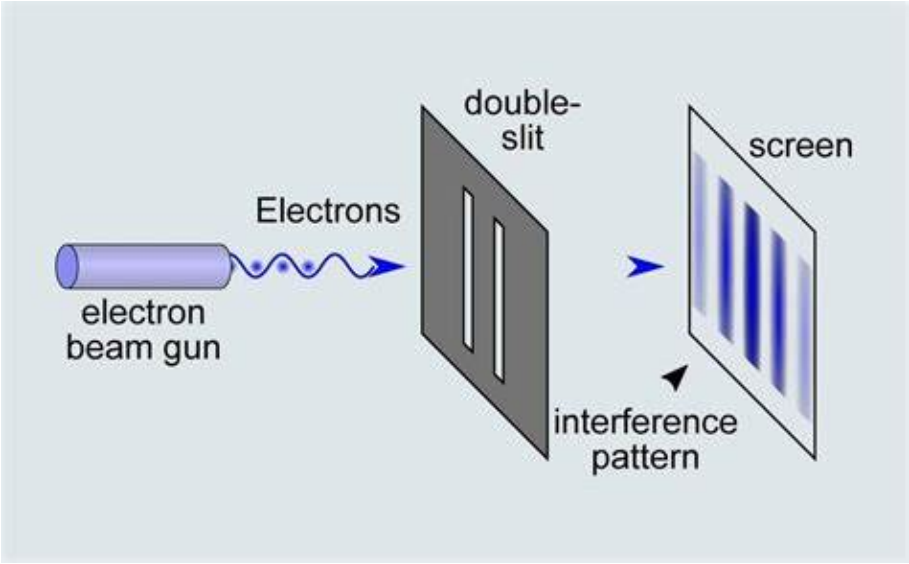

Figure 3: Schematic setup of the double-slit experiment
(Source: https://naturenoon.com/double-slit-experiment-simple/)

2.3 Setup of the experiment

Following the discussion of two fundamental effects from quantum mechanics and general relativity, the focus now shifts to the conceptual foundation of the experimental setup. As highlighted in the introduction, both theories have been remarkably successful within their respective domains, yet physicists have thus far been unable to develop a unified framework that consistently incorporates both. Various theoretical and experimental approaches have been pursued to bridge this gap.

One theoretical approach is string theory [8], which aims to unify quantum mechanics and general relativity within a consistent mathematical framework. On the experimental side, one promising method to probe the limits of quantum mechanics is to perform double-slit experiments with increasingly larger particles [9]. By extending quantum interference experiments to macroscopic scales, researchers seek to identify whether there exists a fundamental boundary where quantum mechanics ceases to hold and classical behavior, as described by general relativity, takes over. This naturally leads to the fundamental question: Where does quantum mechanics end, and where does general relativity begin?

Despite significant progress, a definitive answer remains elusive. It is even conceivable that the unification of these two theories may not be possible. Nevertheless, experimental approaches continue to be crucial for testing the limits of our current understanding and exploring potential deviations from established theories.

This master thesis presents an alternative experimental approach. Instead of using a traditional double-slit experiment, this setup implements a fiber-based Mach-Zehnder interferometer (MZI) to investigate the influence of gravity on quantum superposition. In the final configuration, the two arms of the MZI will be positioned at different heights, introducing a variation in gravitational potential. The earth itself acts as the massive object responsible for inducing the gravitational phase shift, commonly referred to as the Shapiro delay. Photons in a quantum superposition will be sent through the MZI, allowing for an investigation of how they interact with the different gravitational potentials in each arm.

Achieving this goal requires overcoming several experimental challenges. Numerous intermediate steps must be carried out to construct, optimize, and stabilize the interferometer before the final experiment can be performed. The following sections will outline the step-by-step development of the fiber-based Mach-Zehnder interferometer, beginning with its fundamental design and operational principles.

2.3.1 Mach-Zehnder interferometer

A Mach-Zehnder interferometer (MZI), as depicted in Fig. 4, is an essential optical instrument used to measure phase differences with high precision [10]. The fundamental principle of operation is based on the interference of light beams that travel along different optical paths.

In a typical setup, a coherent light beam is directed onto a beam splitter, which divides the beam into two separate paths. Ideally, 50 % of the light is transmitted, while 50 % is reflected. The two beams then propagate along distinct paths where they are reflected by mirrors before being recombined at a second beam splitter. At this point, the overlapping beams interfere, and the resulting intensity is detected at two separate output ports.

The interference pattern observed at the detectors is directly influenced by the relative phase shift ϕ between the two paths. If there is a difference in optical path length, this results in a measurable phase shift, which alters the detected intensity at the output ports. The ability to measure these phase shifts with extreme sensitivity makes the Mach-Zehnder interferometer an invaluable tool in various precision measurements.

This capability has been extensively utilized in gravitational wave detection, where interferometers with significantly extended arms have been employed to measure distortions in spacetime caused by passing gravitational waves. This approach was instrumental in the first direct detection of gravitational waves, an achievement that was honored with the 2017 Nobel Prize in Physics [11].

Despite its fundamental simplicity, the Mach-Zehnder interferometer remains a cornerstone in quantum optics, precision metrology, and gravitational physics, making it an ideal tool for investigating the interplay between quantum mechanics and general relativity in this experimental setup.

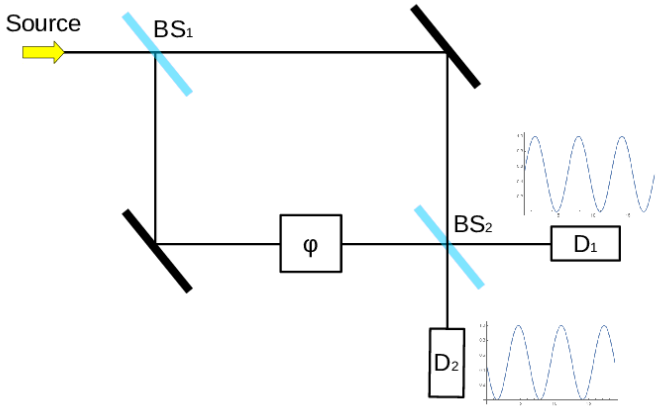

Figure 4: Schematic setup of a Mach-Zehnder interferometer
(Source: https://www.researchgate.net/figure/Schematic-representation-of-Mach-Zehnder-interferometer-fig1-327134479)

In addition to the Mach-Zehnder interferometer, other interferometric configurations exist, such as the Michelson interferometer, depicted in Fig. 5. The Michelson interferometer operates on a similar principle, utilizing beam splitters and mirrors to create interference patterns. However, a fundamental distinction lies in its optical architecture.

Unlike the Mach-Zehnder interferometer, which fully separates the two optical paths and recombines them at a second beam splitter, the Michelson interferometer is partially reflective. A portion of the incoming light is reflected back towards the input source [12]. This reflection can introduce undesired feedback into the laser source, potentially leading to instability and noise. Such back-reflections can be particularly problematic in high-precision measurements, as they degrade the signal quality and reduce the accuracy of phase measurements.

Due to this limitation, Michelson interferometers are more susceptible to optical noise compared to Mach-Zehnder interferometers. This noise sensitivity is a critical factor when selecting an interferometric setup for specific applications. In the context of this experiment, where precise control of phase stability is essential, the Mach-Zehnder configuration is preferred, as it inherently minimizes optical feedback and maintains greater stability.

A more detailed discussion on the impact of optical noise and mitigation strategies will be provided in later sections, where the optimization of the experimental setup is addressed.

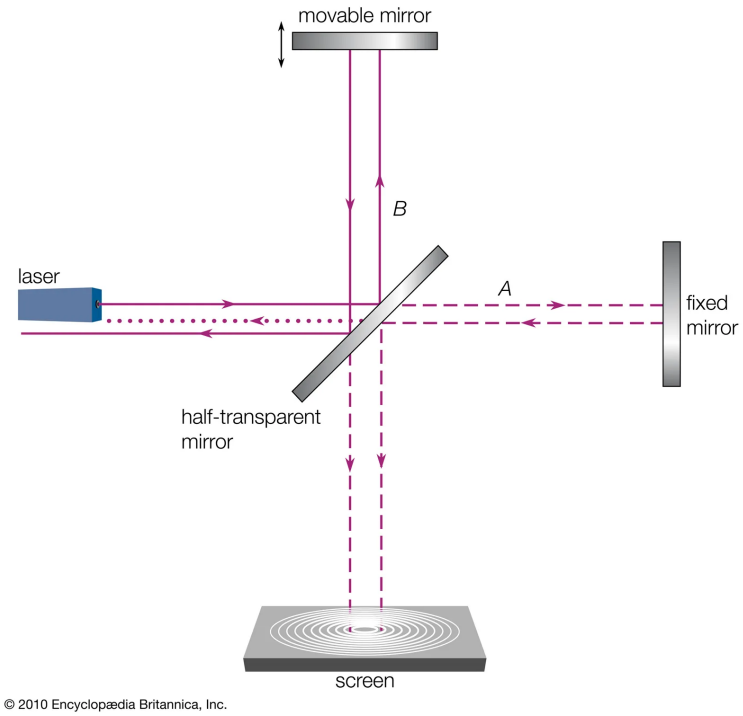

Figure 5: Schematic setup of a Michelson interferometer
(Source: https://www.britannica.com/science/Michelson-Morley-experiment)

2.3.2 Components of fiber interferometry

In this experimental setup, fiber interferometry is employed, meaning that light from a laser source is transmitted through optical fibers to reach the detectors (see Fig.6). Fiber-based interferometers provide several advantages over free-space optical interferometers, including enhanced stability, compactness, and reduced sensitivity to environmental disturbances such as vibrations and air fluctuations. These properties make them particularly suitable for high-precision measurements. This section discusses the key components of a fiber-based Mach-Zehnder interferometer (MZI) and their respective functions within the system.

The fundamental components of the fiber-based MZI include:

- **Laser source:** Provides a coherent optical signal, serving as the input for the interferometric system. The choice of laser source significantly impacts the stability and signal-to-noise ratio of the system. The coherence length of the laser must be sufficiently long to ensure stable interference over the optical path difference in the interferometer. Furthermore, intensity fluctuations and phase noise must be minimized to maintain high-precision phase measurements.

- **Optical fiber:** Guides the light through the system, ensuring controlled propagation with minimal loss. To efficiently guide light through the system, standard telecommunication-grade optical fibers are typically used due to their low attenuation and high transmission efficiency. The refractive index of the fiber directly influences the optical path length, which must be carefully considered when analyzing phase shifts.

- **Fiber-optic couplers:** Fiber-optic couplers function as beam splitters in fiber-based interferometers, directing portions of the optical signal into different paths. These couplers are available with various splitting ratios, ranging from 1:99 (where one output receives 99% of the power and the other receives 1%) to 50:50 (equal power distribution). The choice of splitting ratio depends on the specific experimental requirements, particularly in optimizing interference visibility.

- **Detectors:** Measure the intensity of the recombined optical signal and convert it into an electrical signal for analysis. High-performance photodetectors are used to measure the intensity of the recombined optical signals. The selection of appropriate detectors depends on parameters such as responsivity, wavelength sensitivity, and low-noise characteristics. High-quality detectors are available for all commonly used wavelengths, ensuring compatibility with both the laser source and fiber optics.

The proper selection and optimization of these components are essential for achieving a highsignal-to-noise ratio, maximizing interference visibility, and ensuring the stability of phase measurements in the experiment. As environmental factors such as temperature fluctuations and mechanical vibrations can introduce unwanted noise, additional stabilization techniques may be required, which will be discussed in later sections.

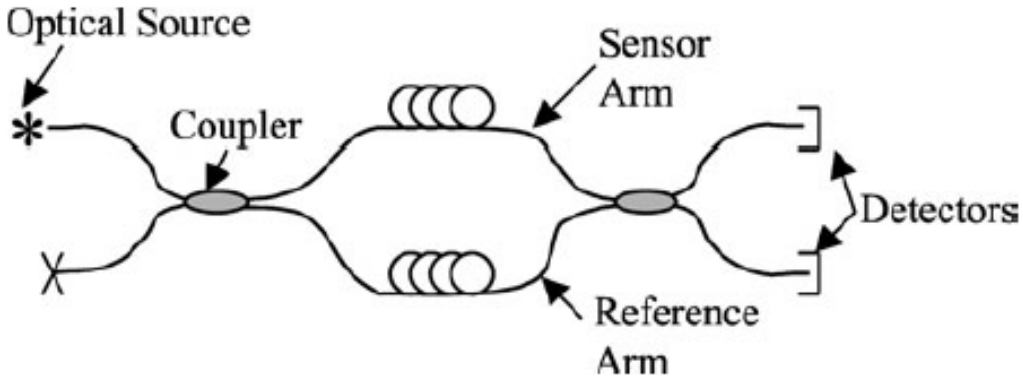

Figure 6: Schematic setup of the fibre-optic MZI
(Source: [13])

2.3.3 Phase shift $\Delta\phi$

The phase shift $\Delta\phi$ between the sensor arm and the reference arm in a fiber-based Mach-Zehnder interferometer (MZI) is a critical parameter for interference-based measurements. The theoretical framework for this phase shift is outlined in the work of C. K. Kirkendall and A. Dandridge [13].
Assuming that the coherence length of the laser source is significantly greater than the optical path difference, i.e.,

$$L_C \gg n(L_R - L_S), \tag{2}$$

where
- L_C is the coherence length of the laser,
- n is the effective refractive index in the optical fiber,
- L_R and L_S are the physical path lengths of the reference and sensor arms,
the signals at the two detectors can be expressed as:

$$I_1 = I_R + I_S + 2\sqrt{I_R I_S}\cos(\phi_R - \phi_S), \tag{3}$$

$$I_2 = I_R + I_S - 2\sqrt{I_R I_S}\cos(\phi_R - \phi_S). \tag{4}$$

Here,
- I_R and I_S denote the optical intensities in the reference and sensor arms,
- ϕ_R and ϕ_S are the optical phase delays in the reference and sensor paths.

The optical intensities are determined by the splitting ratios of the couplers as well as optical losses within the interferometer. The optical phase delay in each arm is given by:

$$\phi = nkL, \tag{5}$$

Where n is the refractive index of the fiber and k is the optical wavenumber, defined as

$$k = \frac{2\pi}{\lambda}, \tag{6}$$

and L is the physical path length.
A more general representation of the detector signal, which will be used throughout this work, is:

$$I_{1,2} = I_0\left(1 \pm V\cos(\Delta\phi)\right), \tag{7}$$

Where I_0 is the average optical power, given by

$$I_0 = I_R + I_S, \tag{8}$$

V is the visibility of the interference pattern, defined as

$$V = \frac{I_{\max} - I_{\min}}{I_{\max} + I_{\min}} = \frac{2\sqrt{I_R I_S}}{I_R + I_S}, \tag{9}$$

with $\Delta\phi$ represents the optical phase difference between the two arms of the interferometer, given by

$$\Delta\phi = \phi_R - \phi_S. \tag{10}$$

This formulation allows precise determination of phase variations in fiber-optic interferometers, which is essential for high-sensitivity applications such as quantum optics and gravitational phase shift measurements.

2.3.4 Polarization

Light can be fundamentally described as an electromagnetic wave [14], consisting of oscillating electric and magnetic fields that propagate through space. The orientation of these oscillations defines the polarization state of the light wave. In general, light can be linearly, circularly, or elliptically polarized, depending on the relative phase and amplitude of the oscillating electric field components.

In the case of linear polarization, the electric field oscillates in a fixed direction, perpendicular to the propagation axis of the beam. The magnetic field is always perpendicular to both the electric field and the direction of propagation, maintaining the characteristic orthogonality of electromagnetic waves (fig.:7).

For circular polarization, the electric field vector rotates in a helical motion as the wave propagates. This occurs when two perpendicular electric field components of equal amplitude are 90° out of phase with respect to each other. The rotation can be left-handed or right-handed, depending on the relative phase shift between the components (fig.:8).

Elliptical polarization represents a more general case, where the electric field vector also rotates, but with varying amplitudes along different axes. This results in an elliptical trajectory of the electric field over time, distinguishing it from the uniform helical motion of circularly polarized light. The degree of ellipticity depends on the relative amplitudes and phase differences between the perpendicular electric field components.

Polarization plays a crucial role in many optical and quantum experiments, as it influences the interaction of light with optical components, including beam splitters, waveplates, and interferometers. Understanding and controlling polarization is essential for optimizing visibility in interference experiments and minimizing unwanted phase distortions in precision optical measurements.

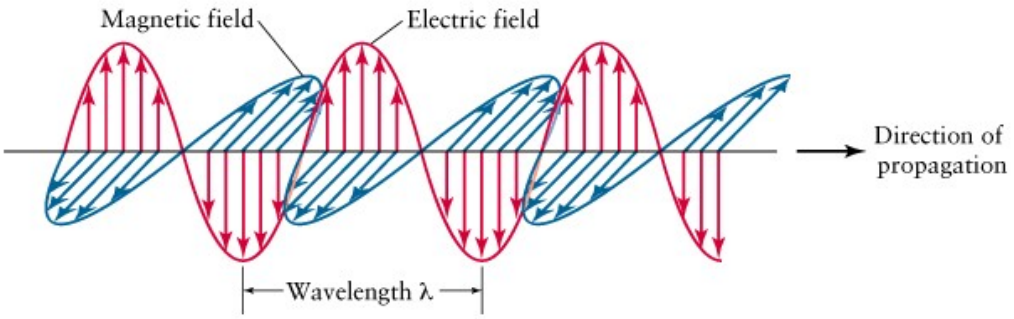

Figure 7: Linear polarization of light
(Source: https://wisp.physics.wisc.edu/astro104/lecture6/lec6-print.html)

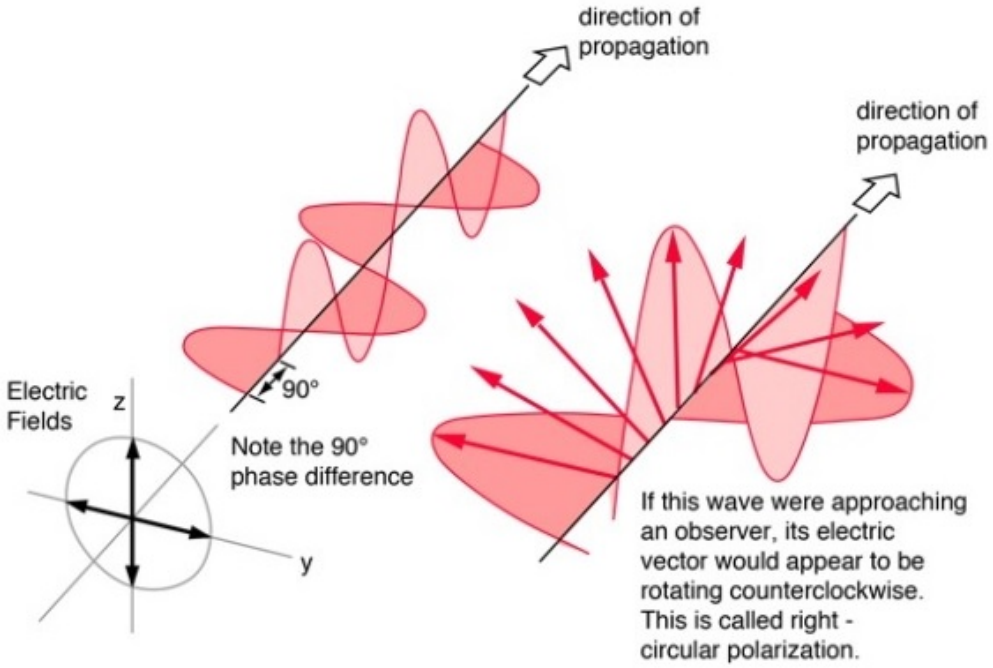

Figure 8: Circular polarization of light
(Source: https://physicsopenlab.org/2019/08/20/polarization-of-light/)

Polarization plays a important role in this experimental setup, as the interference pattern observed at the output strongly depends on the polarization states of the recombined signals. When the two optical signals are perfectly aligned in polarization, they interfere constructively or destructively, resulting in maximum visibility of the interference pattern. Conversely, if the polarization states of the two beams are orthogonal, no interference occurs, leading to a complete loss of visibility.

To ensure optimal interference conditions, the experimental setup includes a polarization control stage in one of the interferometer arms. This stage compensates for any polarization drift introduced by the fiber optics and ensures that the recombined signals maintain a high degree of coherence. By actively adjusting the polarization alignment, the visibility of the interference fringes is maximized, improving the sensitivity and accuracy of the phase measurements.

Proper polarization management is particularly critical in fiber-based interferometry, where birefringence effects in the optical fibers can cause unwanted polarization rotations. Addressing these effects ensures stable and reproducible measurements, which are essential for the precision required in this experiment.

2.4 Noise sources in the system

In any high-precision interferometric setup, multiple sources of noise influence the measurement accuracy and system stability. While some noise contributions are negligible, others significantly impact the system's performance and must be carefully managed. Among the most critical noise sources in this experiment are laser phase noise and fiber thermal noise, both of which introduce phase instabilities in the interferometric signal.

2.4.1 Laser phase noise

Laser phase noise [13] is one of the fundamental noise sources in any interferometric setup. It arises due to fluctuations in the optical frequency of the laser source, which translate into phase noise in the interferometer. The magnitude of this effect depends on the laser linewidth and the optical path mismatch between the interferometer arms. A narrow-linewidth laser is therefore preferred to minimize frequency fluctuations and maintain phase stability.
Figure 9 illustrates the frequency noise characteristics of three commonly used lasers, alongside the corresponding phase noise induced in an interferometer with a 1 m path mismatch between the reference and sensing arms. The choice of laser is crucial in ensuring that laser phase noise remains below the fundamental noise limits imposed by the interferometers design.

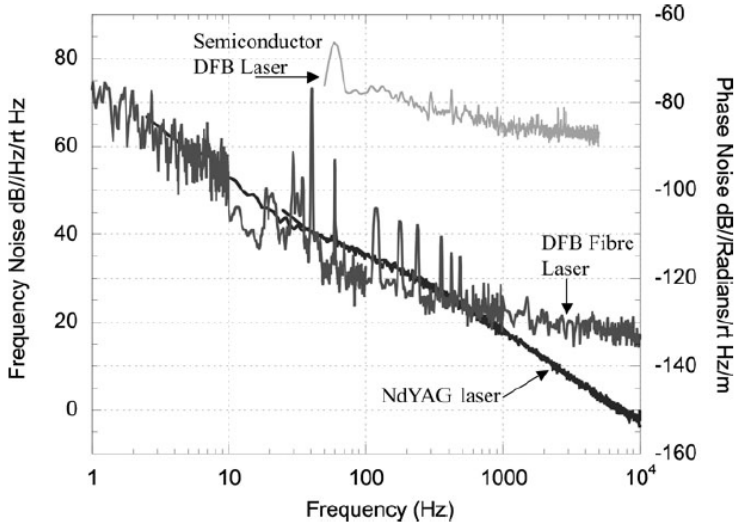

Figure 9: Laser frequency noise for a 1319 nm Nd:YAG laser, a 1550 nm DFB-EDFL, and a 1550 nm semiconductor DFB laser.
(Source: [13])

2.4.2 Fiber thermal noise

As the optical fiber length increases, fiber thermal noise becomes a dominant limitation. This noise originates from thermally induced fluctuations in the optical path length due to variations in the fibers refractive index and mechanical expansion. The intrinsic fiber thermal noise can be approximated by:

$$\text{Thermal noise} \approx (-147 + 10 \log L) \text{ dB re rad} \cdot \text{Hz}^{-1/2} \quad \text{at 1 kHz}, \tag{11}$$

where L is the total fiber length in meters [13]. The noise contribution decreases with increasing frequency but remains significant at low frequencies.
For an interferometric sensor containing 100 m of fiber in both the reference and sensing arms (total fiber length: 200 m), the thermal phase noise limit is approximately:

$$1\,\mu\text{rad} \cdot \text{Hz}^{-1/2} \quad \text{at 1 kHz}. \tag{12}$$

This makes fiber thermal noise one of the most significant sources of phase instability in the system.

2.4.3 Other noise sources and system limitations

In addition to laser phase noise and fiber thermal noise, several other factors contribute to the overall noise in the system:

- Electronic noise: Introduced by amplifiers, power supplies, and signal processing electronics.
- Detector noise: Arises from dark current, shot noise, and thermal fluctuations in the photodetectors.
- Environmental noise: Includes mechanical vibrations, acoustic noise, and temperature variations affecting fiber stability.

Each of these noise sources contributes to the fundamental measurement limit of the interferometric system. To reduce these effects, several approaches can be implemented, such as thermal shielding of the interferometer arms and vibration isolation. However, since it is impossible to eliminate all noise sources, an active feedback control mechanism is introduced into the setup. This feedback loop dynamically compensates for phase fluctuations, improving system stability and extending the measurement sensitivity.

2.5 Feedback-Loop

The fundamental concept of a feedback loop [15] is to utilize the system?s output as an input correction signal to regulate performance and minimize errors. Feedback loops are widely used in control systems to stabilize signals, enhance system response, and suppress noise. There are two principal types of feedback mechanisms: positive feedback and negative feedback.

2.5.1 Positive feedback

In a positive feedback system [15], the input and output signals are added together, reinforcing the systems gain. This type of feedback is typically used in applications requiring signal amplification or oscillation generation. A simple example of a positive feedback system is an operational amplifier circuit, as illustrated in Fig.10. In this configuration, a portion of the output voltage is fed back to the non-inverting input through the resistor R_F. As a result, a positive output further enhances itself after feedback, and a negative output intensifies in the opposite direction. This reinforcing effect makes positive feedback useful for signal regeneration but can lead to instabilities if not properly controlled.

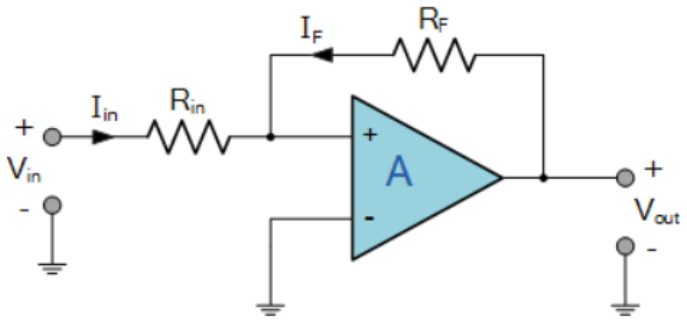

Figure 10: Basic positive feedback system.
(Source: https://www.electronics-tutorials.ws/systems/feedback-systems.html)

2.5.2 Negative feedback

In contrast, negative feedback systems [15] subtract the output signal from the input, thereby reducing the overall system gain and increasing stability. This configuration is particularly advantageous for precision applications, where signal stabilization is essential.
A negative feedback loop can also be implemented using an operational amplifier, as shown in fig.11. In this setup, the output signal is fed back to the inverting input, counteracting fluctuations and stabilizing the response of the system.

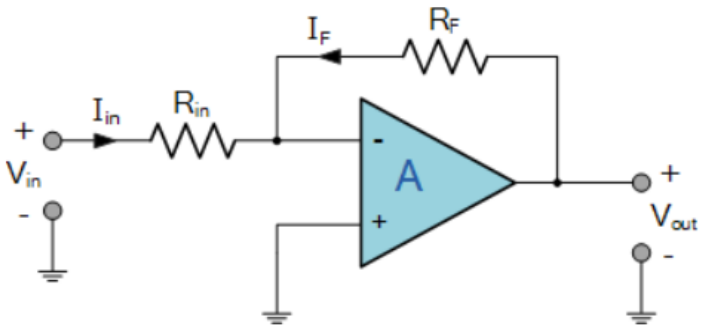

Figure 11: Basic negative feedback system.
(Source: https://www.electronics-tutorials.ws/systems/feedback-systems.html)

Negative feedback is extensively used in signal regulation and noise suppression due to its stabilizing nature. If an external disturbance affects the system output, the negative feedback loop compensates for the variation, maintaining signal integrity. This property makes negative feedback an ideal choice for phase stabilization in the Mach-Zehnder Interferometer (MZI) setup.
In this experiment, an analog feedback loop is implemented to actively control noise and stabilize the phase shift in the interferometric system. The core of this feedback system is a third-order low-pass filter, depicted schematically in fig.12.

Functional Segments of the Feedback Loop:

- Error signal generation: The first amplifier calculates the difference between Input A and Input B while compensating for a predefined bias. Ideally, this sum should be zero, but in practice, fluctuations and noise cause deviations.
- Adjustable resistance for fine-tuning: An adjustable resistor is positioned before the second amplifier. This introduces an additional degree of freedom, allowing the user to fine-tune the signal after the initial amplification stage.
- Integrator for frequency-dependent amplification: The second amplifier functions as an integrator, selectively amplifying signals depending on their frequency characteristics.
- DC offset correction: The final stage incorporates a DC offset adjustment to condition the output signal for further processing.

The implementation of this feedback system ensures active compensation of phase fluctuations, effectively reducing noise and maintaining phase stability within the limits imposed by the experimental setup.

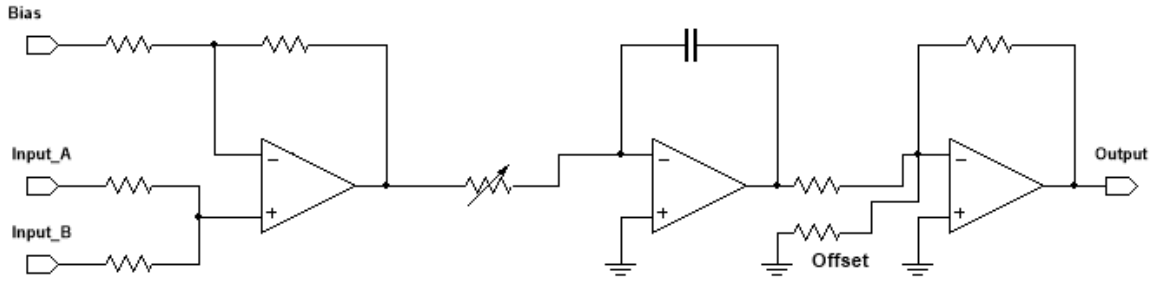

Figure 12: Schematic representation of the analog feedback loop.

3 Experimental setup: MZI with analog feedback loop and fiber stretcher

3.1 First setup: Simple Mach-Zehnder

The initial step in this experiment involved constructing a basic Mach-Zehnder interferometer (MZI) without any additional electronic control. The primary objective of this setup was to characterize fundamental properties of the interferometer, such as visibility and phase stability. Figure 13 presents the schematic layout of the simple fiber-based MZI, which serves as the foundational system for further modifications.

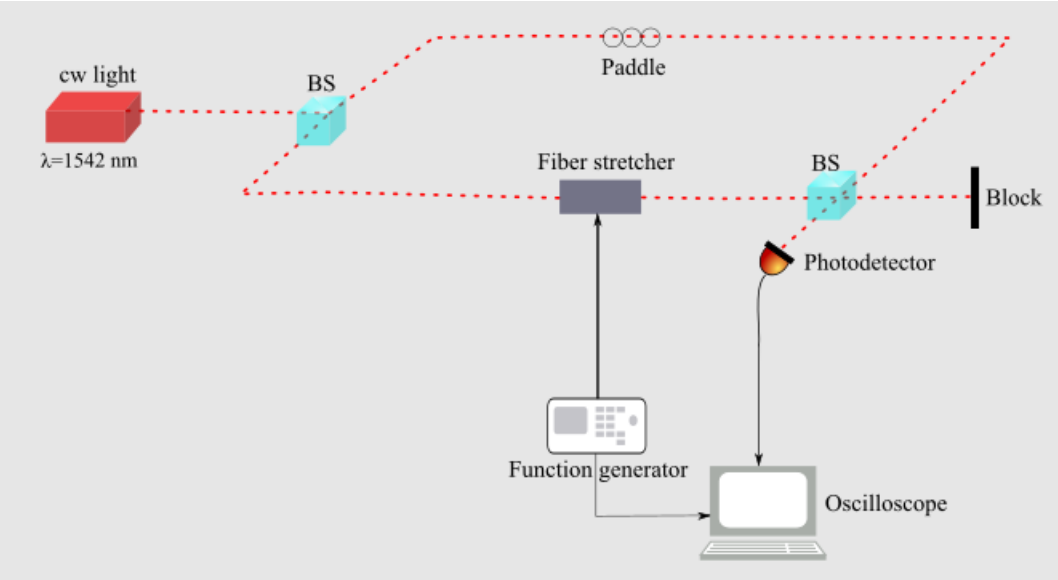

Figure 13: Schematic representation of a simple fiber-based Mach-Zehnder interferometer.

Laser Source: The system employs a continuous-wave laser source [22] with a wavelength of $\lambda = 1542$ nm, corresponding to the infrared spectrum. To facilitate initial system testing, a low-intensity beam was utilized, with an output power of approximately 2 mW. The emitted light exhibits predominantly linear polarization, which is crucial for maintaining high interference visibility.

Optical Fiber System: Unlike conventional free-space interferometers, this MZI is entirely constructed using fiber optics [23]. The use of optical fibers enhances the systems stability, compactness, and robustness by minimizing environmental disturbances such as mechanical vibrations and air fluctuations.

Beam Splitters: To split and recombine the optical paths, 50:50 fiber beam splitters were employed [23]. These beam splitters ensure equal division of optical power between the two interferometer arms, enabling precise interference measurements.

Fiber Stretcher: A fiber stretcher [24] is incorporated into one of the interferometer arms, positioned between the two beam splitters. The fiber stretcher is driven by an external function generator [25], which applies a periodic modulation to the fiber length. This modulation introduces a controlled phase shift into the interferometer, allowing dynamic measurements of phase variations at the output. In this experiment, a sinusoidal waveform was used to induce periodic stretching of the fiber.

Polarization Control (Paddles): To control the polarization state of light propagating through the system, a polarization adjustment unit known as paddles [26] was implemented in one interferometer arm. The polarization unit consists of a half-wave plate and two quarter-wave plates, arranged in a quarter-half-quarter configuration. This setup enables the realization of arbitrary SU(2) polarization transformations [16]. By adjusting the paddle settings, the interference visibility can be maximized or minimized, as discussed in Chapter 2.3.4. In fiber-based interferometry, an alternative approach is to position the polarization control unit before the first beam splitter to ensure uniform polarization across both interferometer arms.

Output and Detection: At the output of the interferometer, the two optical beams are recombined using the second 50:50 beam splitter. One of the output ports is blocked, while the other is directed into a high-sensitivity photodetector equipped with an amplifier [27]. The detected signal is then analyzed using an oscilloscope [28], allowing precise measurement of interference patterns and phase shifts.

The construction of this simple MZI serves as an essential preliminary step for understanding and optimizing the interferometric response before implementing advanced stabilization techniques. By characterizing the systems basic properties such as visibility, phase stability, and polarization effects this setup provides a foundation for further improvements, including feedback control mechanisms and precision phase stabilization.

3.1.1 Experimental setup

Figures 14 and 15 present the experimental implementation of the fiber-based Mach-Zehnder interferometer (MZI) at laboratory scale. The setup consists of several key components, each playing a crucial role in the functionality and measurement accuracy of the interferometer.
The following list provides an overview of the main components integrated into the system:

1. **Incoming Laser:** Provides the coherent optical source for the interferometric measurements.
2. **Beam Splitter 1:** Splits the incoming laser beam into two optical paths.
3. **Fiber Stretcher:** Introduces a controlled phase shift in one arm of the interferometer.
4. **Polarization Stage:** Adjusts the polarization state of the optical signal to optimize interference visibility.
5. **Beam Splitter 2:** Recombines the two optical paths, enabling interference effects to be observed.
6. **Photodetector + Amplifier:** Converts the optical interference signal into an electrical signal for further analysis.
7. **Power Meter:** Measures the optical power in the system for calibration and alignment verification.
8. **Oscilloscope:** Records and visualizes the interference signal for phase shift analysis.
9. **Function Generator:** Provides an external modulation signal to the fiber stretcher, enabling dynamic phase modulation.

The laboratory setup is designed to provide a stable environment for conducting precise interferometric measurements. The use of fiber optics minimizes external disturbances such as mechanical vibrations and air fluctuations, ensuring high phase stability. Additionally, the polarization stage allows for fine-tuning of interference visibility, which is essential for accurate phase shift measurements.

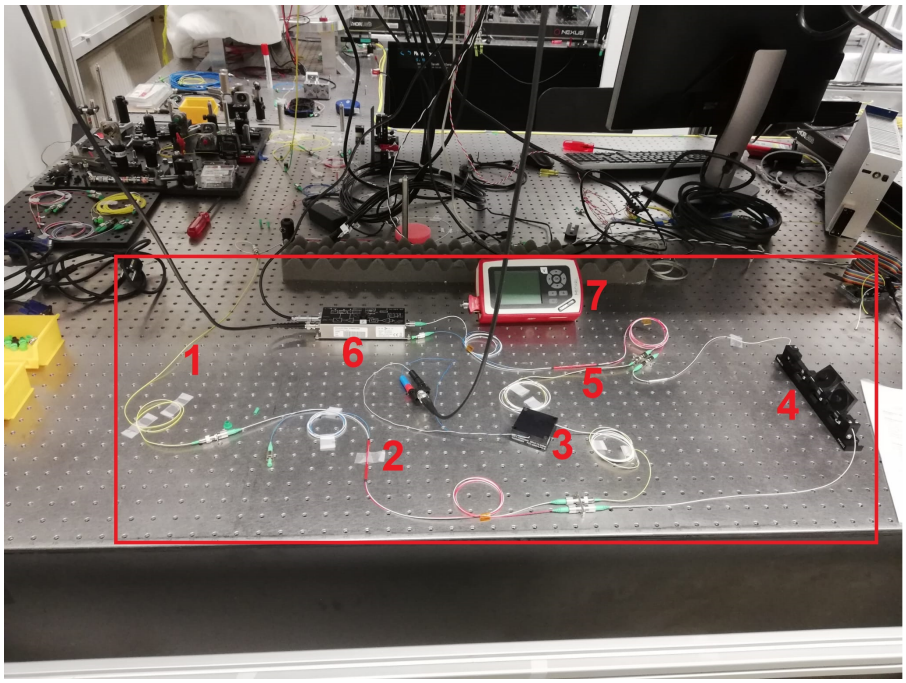

Figure 14: Experimental setup of the fiber-based Mach-Zehnder interferometer.

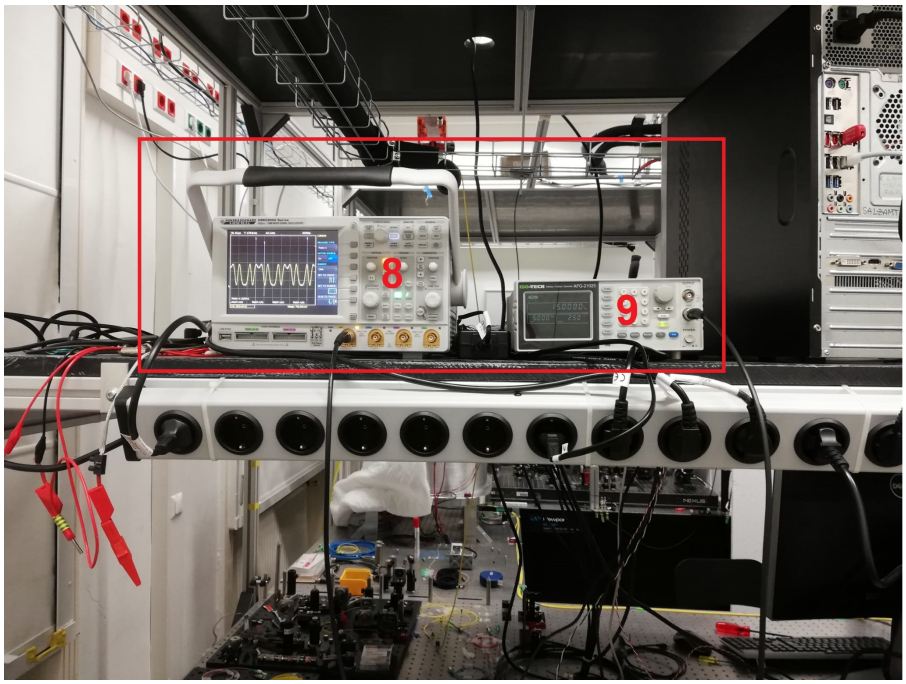

Figure 15: Alternative perspective of the fiber-based Mach-Zehnder interferometer setup.

The successful implementation of this experimental setup provides the foundation for further optimization, including feedback control mechanisms and extended phase stabilization techniques.

3.1.2 Measurement

To assess the efficiency of the interferometric setup, the power loss of the laser throughout the system was measured. This required measuring the optical power at various critical points within the interferometer. Additionally, the maximum achievable visibility of the interference fringes was determined. All measurements presented in this section were conducted using a calibrated power meter [29].

For a better understanding of the measurement locations, the corresponding measuring points are marked in fig.16.

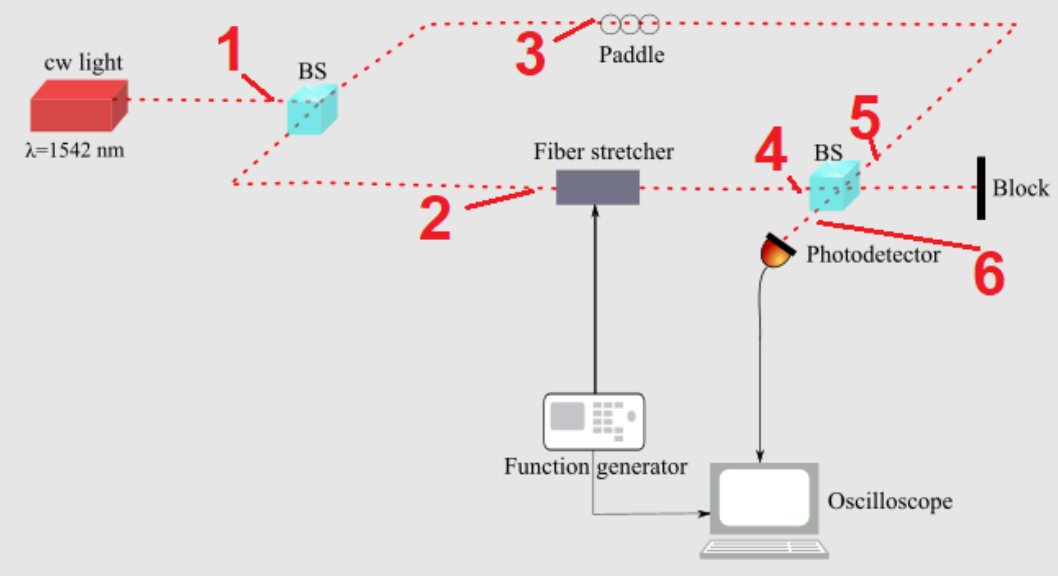

Figure 16: Measurement points within the interferometric setup.

Power loss analysis:

The following measurements provide a quantitative evaluation of optical power loss at different stages of the interferometer:

1, Input power: The initial laser power before entering the system is 2,093 mW.

2+3, Power in interferometer arms: Optical power in the arm containing the fiber stretcher is 1,064 mW. Optical power in the arm containing the polarization stage is 0,981 mW. That gives in total 2,045 mW, which is a power loss of approximately 2 % due to the beam splitter and initial fiber transmission losses.

4+5, Power before recombination: Optical power in the arm with the fiber stretcher is 1,046 mW. Optical power in the arm with the polarization stage is 0,890 mW. That gives in total 1,936 mW, which is a power loss of approximately 8 % within the arms.

6, Power after recombination: The total power measured after recombining both interferometer arms is 1.658 mW. Indicating an overall power loss of approximately 20 % throughout the entire system.

The observed power loss is attributed to insertion losses of the fiber components, beam splitters, and general attenuation within the optical fibers. This level of loss is consistent with standard fiber-based interferometric setups.

Visibility measurement without fiber stretcher

The next step involved determining the visibility of the interference fringes. The visibility was first measured without the fiber stretcher and function generator, allowing for an evaluation of the intrinsic interferometer performance.
To measure visibility, the maximum and minimum detected optical power after interference were recorded. The polarization paddles were adjusted to maximize and minimize the output signal, respectively.
Visibility is calculated using the standard formula:

$$V = \frac{P_{\max} - P_{\min}}{P_{\max} + P_{\min}} \tag{13}$$

The measured power values at the two output ports of the interferometer (see Fig. 14) are as follows:

- **First Output (White Port)**
  - $P_{\max} = 1.638$ mW
  - $P_{\min} = 0.020$ mW
- **Second Output (Blue Port)**
  - $P_{\max} = 1.506$ mW
  - $P_{\min} = 0.077$ mW

This results in the following visibility values:

- **First Output:** $V = 98\%$
- **Second Output:** $V = 91\%$

Since the first output exhibits a higher visibility, it was selected for all subsequent measurements.

Visibility Measurement With Fiber Stretcher

The same measurement procedure was repeated with the fiber stretcher and function generator activated, introducing a controlled phase modulation. The function generator was configured with the following parameters:

- **Waveform:** Sinusoidal wave
- **Frequency:** $f = 20$ kHz
- **Peak-to-Peak Voltage:** $V_{pp} = 5$ V

Under these conditions, the calculated visibility was approximately 95 %, which is a typical value in fiber-based interferometry.
This measurement confirms that the introduction of an external phase modulation does not significantly degrade the interference visibility, ensuring the system's robustness for further experimental investigations.

3.2 Second setup: Fiber stretcher + analog feedback loop

The first step towards improving the stability and performance of the fiber-based Mach-Zehnder interferometer (MZI) is the integration of a feedback loop. The schematic representation of the enhanced interferometric setup, incorporating the feedback mechanism, is shown in fig.17.

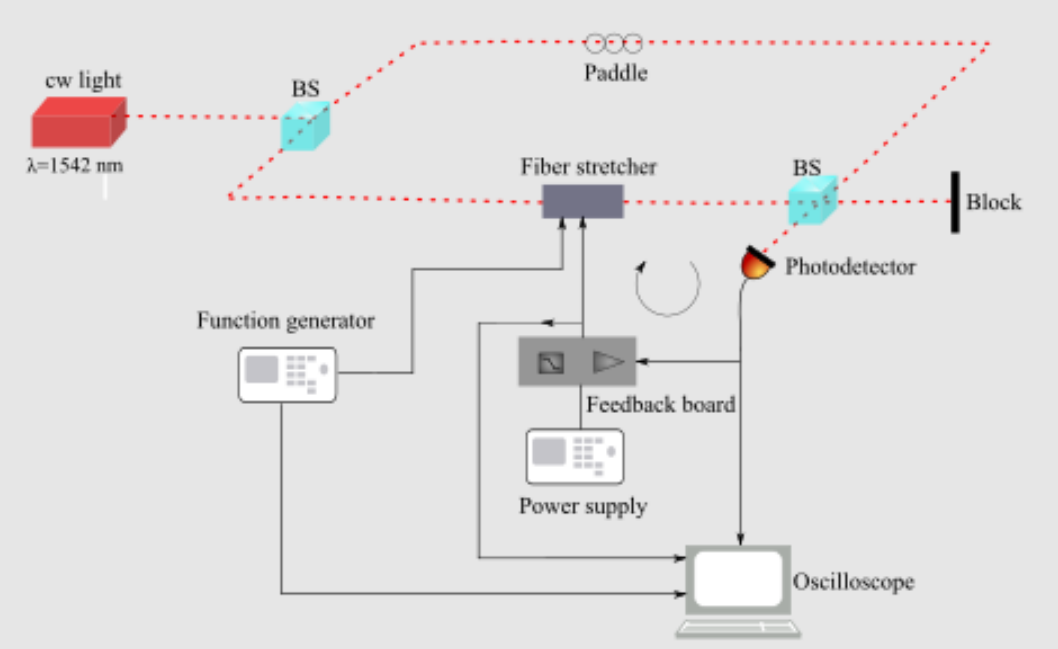

Figure 17: Implementation of a feedback-controlled fiber-based Mach-Zehnder interferometer.

As discussed in Chapter 2.5, the output signal of the Mach-Zehnder interferometer is used as an input to the fiber stretcher through a dedicated feedback board. The purpose of this feedback mechanism is to actively compensate phase fluctuations and minimize the impact of noise sources.

The feedback board processes the interferometric signal and generates a correction signal that modulates the fiber stretcher. A separate power supply [30] is required to operate the feedback control system. By implementing this control mechanism, it becomes possible to reduce noise-induced phase instabilities in the system, even without explicitly identifying the individual noise sources.

This first iteration of the improved setup enables partial stabilization of the interferometric phase, allowing for an initial level of noise suppression. However, the ultimate limitations of this approach and the extent to which noise sources can be mitigated will be further explored in Chapter 3.3, where an advanced version of the setup is evaluated.

3.2.1 Experimental setup

At the laboratory scale, the implementation of the feedback loop (as shown in Chapter 2.5.2) can be observed in fig.18 and fig.19. The feedback system is realized through a printed circuit board (PCB), which serves as the core of the stabilization mechanism [31]. The integration of this PCB-based feedback system enables real-time correction of phase fluctuations, improving the stability and reliability of the interferometer.
The key components of the feedback loop setup include:

1. **Output Signal Feedback:** The interference signal from the Mach-Zehnder interferometer is fed back to the fiber stretcher through the feedback control circuit.

2. **Feedback Board:** The PCB processes the detected signal and generates a correction signal that modulates the fiber stretcher, actively stabilizing the interferometric phase.

3. **External Power Supply Connection:** The feedback system requires a dedicated power source to operate efficiently, ensuring a stable and continuous phase correction mechanism.

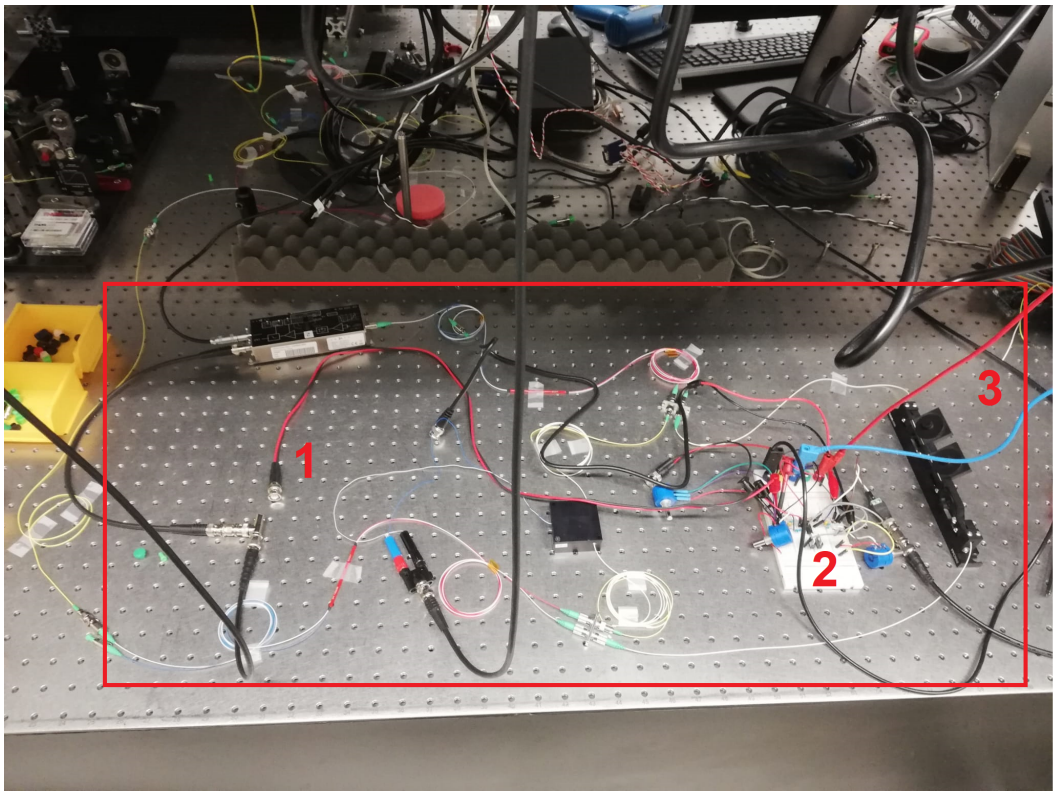

Figure 18: Laboratory implementation of the improved Mach-Zehnder interferometer with integrated feedback board.

The integration of the feedback system marks a significant improvement in the experimental setup, as it allows active phase stabilization, reducing unwanted noise and improving measurement accuracy. By dynamically adjusting the fiber stretcher, the system compensates for external perturbations that would otherwise introduce phase drifts in the interferometric signal.

The PCB board used for feedback control is depicted in fig.19. This board is designed to process the interferometric signal with high precision, ensuring that the generated correction signal maintains optimal phase stability.

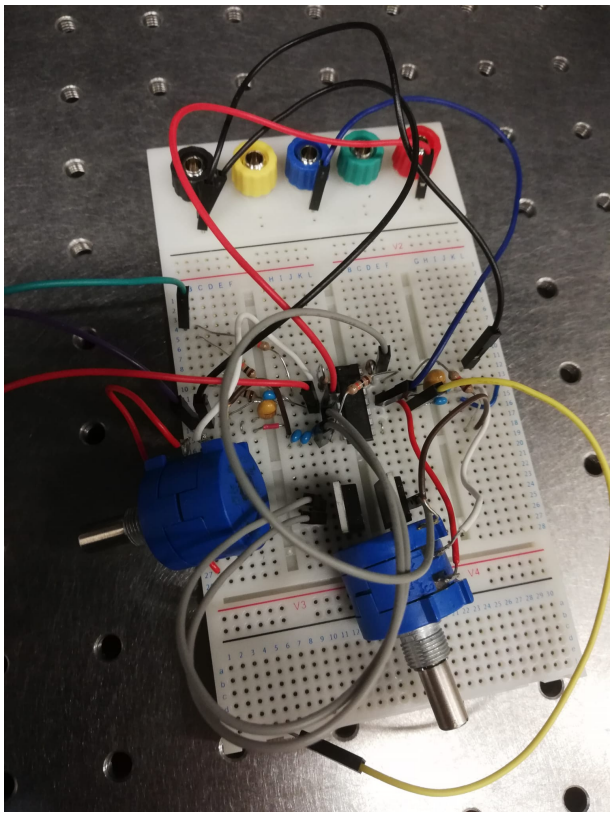

Figure 19: Printed circuit board (PCB) used for the feedback control mechanism.

This real-time phase correction approach represents a crucial step towards minimizing phase noise, thereby enhancing the overall performance of the fiber-based Mach-Zehnder interferometer. Further optimizations, such as refining the feedback control algorithm and reducing residual noise sources, will be explored in subsequent experimental stages.

3.2.2 Measurement

With the successful implementation of the feedback board, it became possible to actively control and stabilize the interferometric phase. The system demonstrated long-term stability, meaning that the phase remained locked over time without observable drift on the oscilloscope. This represents a significant improvement, ensuring that phase fluctuations induced by environmental noise and system instabilities are effectively suppressed.

Measurement of the Phase-Voltage Relationship ϕ/V

A crucial characteristic of any interferometer is its phase response to applied voltage (ϕ/V). This parameter determines how effectively an applied voltage can modulate the phase within the interferometer and is essential for precise phase control.
To measure this response, the interferometric signal was manipulated such that the maxima and minima of the sinusoidal waveform on the oscilloscope aligned at the same amplitude level, as shown in fig.20. At this specific point, the phase shift corresponds exactly to 2π, allowing for a direct determination of the phase-voltage relationship.

The procedure was repeated for multiple voltage values to ensure statistical accuracy. The final result, obtained as the mean of all measured data points, is given by:

$$\frac{\phi}{V} = \frac{2\pi}{6.71V} = (0.936 \pm 0.11)\frac{\text{rad}}{\text{V}} \tag{14}$$

$$\frac{\lambda}{V} = \frac{1542.12\ \text{nm}}{6.71V} = (230 \pm 9)\frac{\text{nm}}{\text{V}} \tag{15}$$

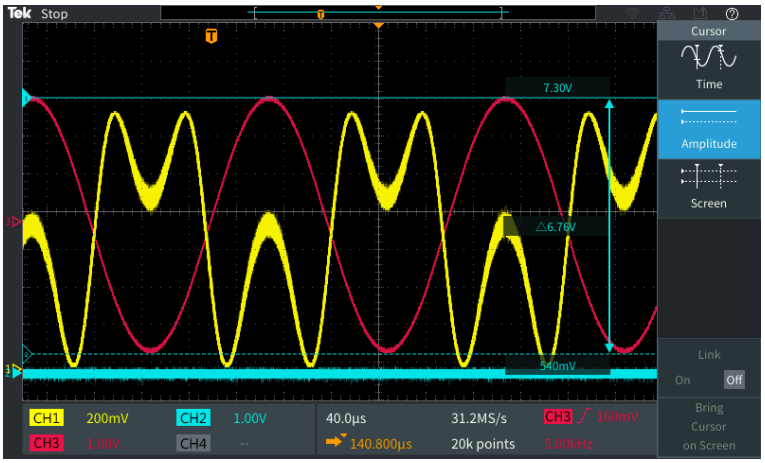

Figure 20: Illustrative example of the interferometric output during phase-voltage calibration.

Achieving active phase stabilization using the feedback board marks a major milestone in the development of the interferometric system. The ability to maintain a locked phase state ensures that the interferometer remains unaffected by slow phase drifts caused by environmental noise, mechanical fluctuations, or temperature variations. This stability is crucial for high-precision applications, particularly in experiments requiring long-term phase coherence.

The next logical step in optimizing the setup is to investigate the limitations of the feedback system. As the length of the fiber arms increases, the associated noise levels also rise, which could pose a challenge for maintaining phase stability. The following section will explore the performance limits of the feedback loop, analyzing how effectively it compensates for noise at increasing fiber lengths and identifying potential strategies for further improvement.

3.3 Third setup: Limit of the feedback board

The next step in optimizing the setup was to assess the limits of the current configuration by progressively increasing the fiber length in one of the interferometer arms, as shown in fig.21. With each extension of the fiber, the interferometer's ability to maintain phase stability and lock decreases, revealing the challenges posed by environmental noise at longer distances.

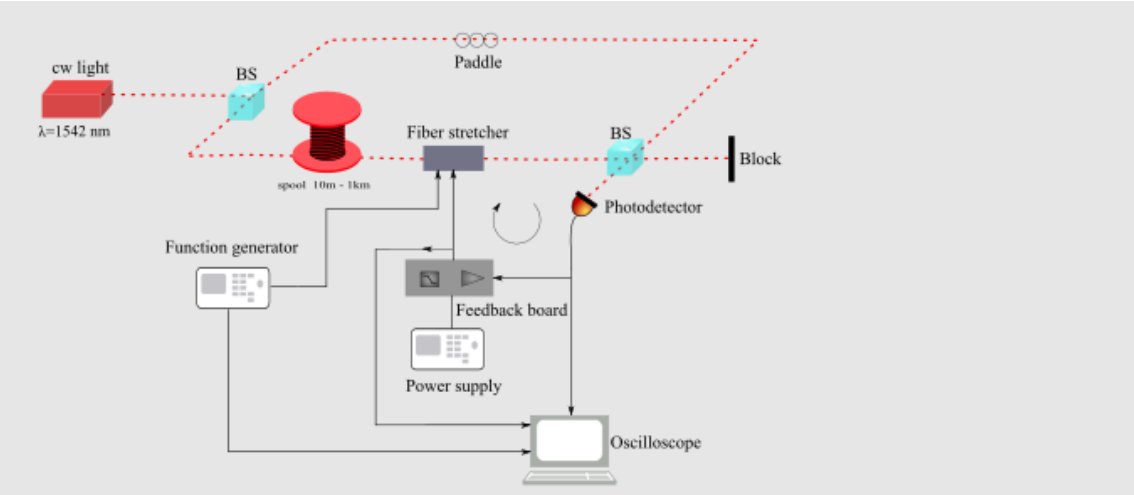

Figure 21: Experimental setup of the fiber-based Mach-Zehnder interferometer with feedback loop and extended fiber spool.

3.3.1 5 m fiber

The first experiment involved extending one arm of the interferometer by 5 meters of optical fiber [23]. The setup, as shown in fig.22, showed that the phase was still relatively stable, although not as stable as without the fiber extension. The output signal displayed some blurriness, indicating that phase stability was slightly compromised, but the system remained locked long enough to allow for measurements. The results are shown in fig.23, where the interferometric signal is still of acceptable quality, though it is affected by small phase fluctuations.

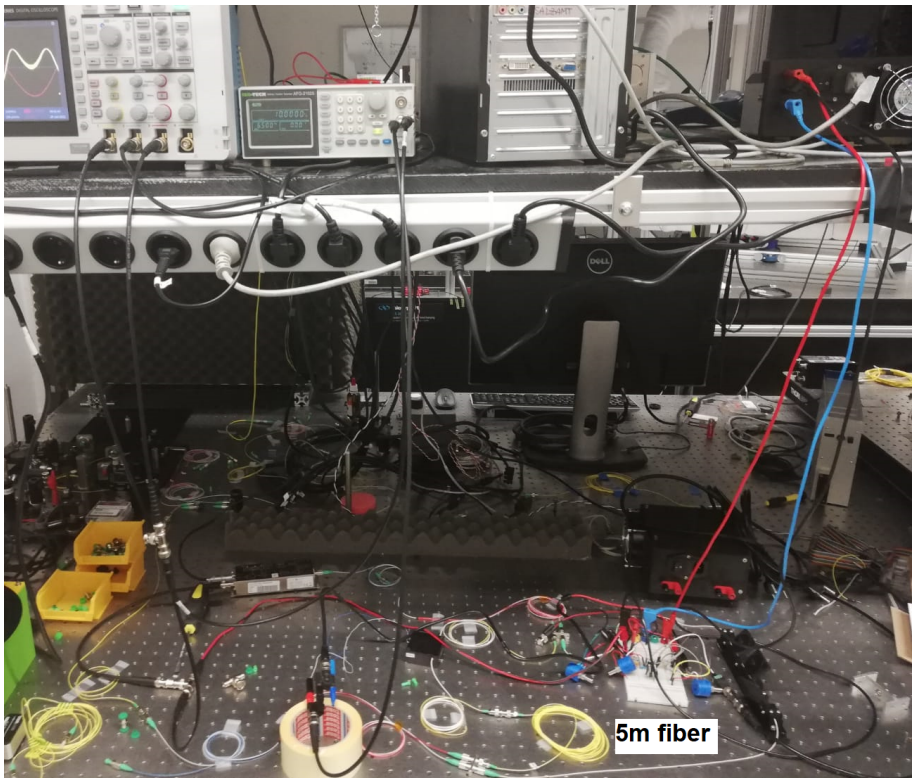

Figure 22: Experimental setup of the Mach-Zehnder interferometer with 5m fiber.

Figure 23: Signal output from the interferometer with 5m fiber.

3.3.2 15 m fiber

Increasing the fiber length to 15 meters (fig.24) resulted in further degradation of phase stability. The output signal became increasingly blurry and the phase lock only lasted for a few seconds, as shown in fig.25. This behavior can be attributed to the increased noise background introduced by the longer fiber length, which is not fully compensated by the feedback loop. The system could no longer maintain a stable phase lock over an extended period.

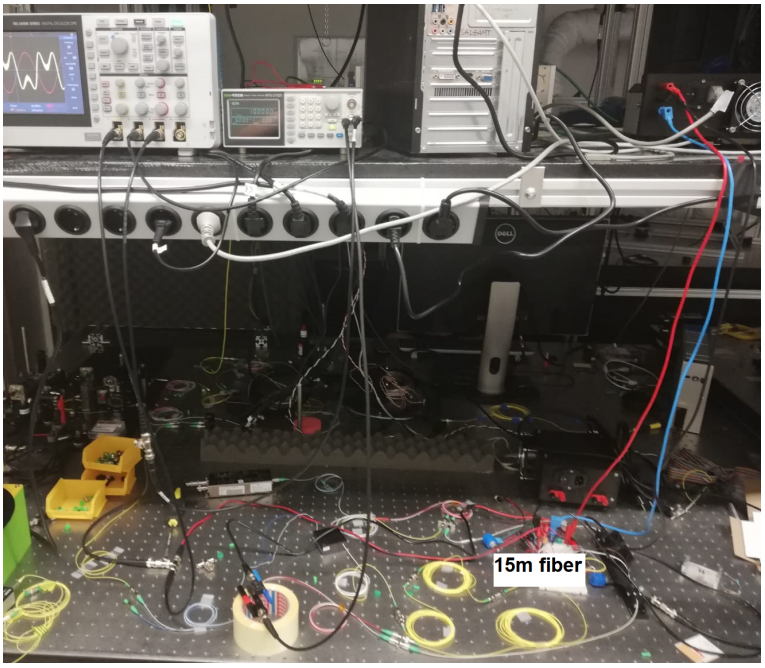

Figure 24: Experimental setup of the Mach-Zehnder interferometer with 15m fiber.

Figure 25: Signal output from the interferometer with 15m fiber.

3.3.3 1 km fiber spool

The final test involved a 1km fiber spool [32], as shown in fig.26. At this length, the noise levels were so amplified that the interferometer could no longer provide any meaningful measurements. The increased noise background completely disrupted the phase lock, and the output signal is no longer usable for precise measurements, as demonstrated in fig.27. The feedback loop was insufficient to stabilize the system under such high noise conditions.

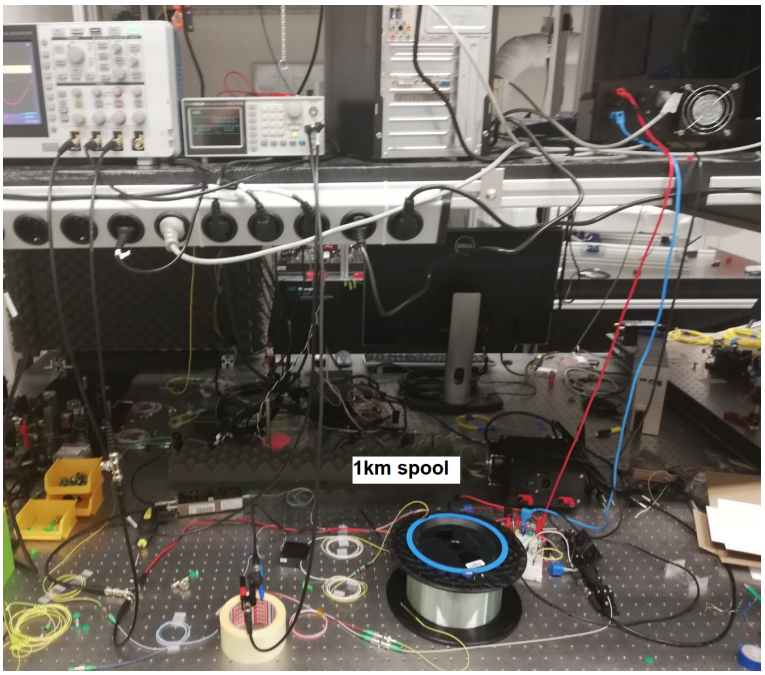

Figure 26: Experimental setup of the Mach-Zehnder interferometer with 1km fiber spool.

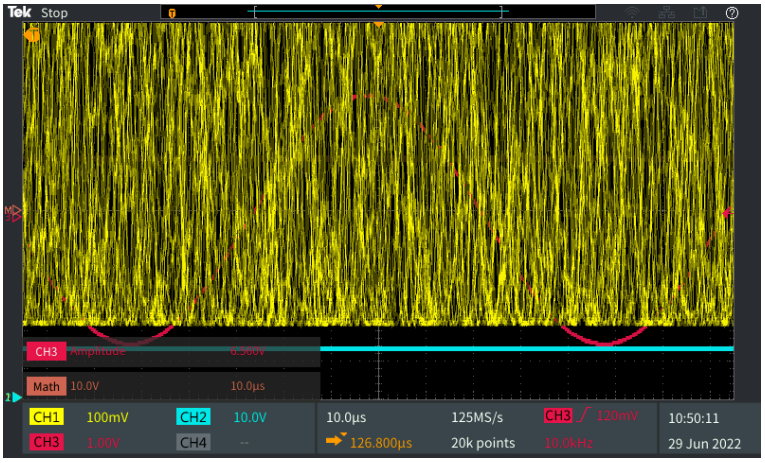

Figure 27: Signal output from the interferometer with 1km fiber.

3.3.4 Shielding techniques and environmental factors

To address the increasing noise levels, shielding techniques were employed to isolate the longer arm of the interferometer from environmental disturbances. Several polystyrene casings were constructed to enclose the fiber, with the aim of minimizing temperature fluctuations and external vibrations. However, these shielding efforts did not lead to any significant improvement in phase stability. Furthermore, testing the system at different times of the day did not reveal any substantial changes in performance, suggesting that external environmental factors were not the primary source of noise.
The next logical step is to further investigate the fundamental limits of the feedback loop, particularly as it relates to handling long fiber lengths and increasing noise levels. The results of these investigations will help determine the ultimate performance bounds of the system and guide potential improvements for future iterations.

3.4 Conclusion so far

In the initial setup, the primary goal was to measure basic characteristics of the interferometer, such as the visibility of the interference fringes. These measurements provided essential insights into the system's performance under ideal conditions.
In the second setup, a feedback loop was introduced to stabilize the phase, aiming to actively lock the phase and reduce the effects of noise. This improvement worked well at the normal laboratory scale, allowing the interferometer to maintain phase stability over extended periods. However, as the fiber arm length was increased, the system's performance began to degrade significantly.
Even with a 15 m fiber, the signal quality diminished rapidly, and the phase lock time became increasingly shorter. This behavior indicates that the feedback loop was unable to fully compensate for the noise background at longer distances. At this point, the system reached its limit, as the interferometer could no longer maintain a stable phase lock over an acceptable period.
Attempts to shield the system from external environmental factors were made, but unfortunately, these efforts did not lead to a significant improvement in performance. The shielding had a minimal effect on reducing noise or stabilizing the phase at longer fiber lengths.
To achieve the desired measurements, which require a fiber arm length of approximately 100 km, a new experimental setup will be necessary. The current systems limitations, both in terms of phase stability and noise suppression, highlight the need for further technological improvements to handle such large-scale distances.

4 Improved setup: MZI with two AOM and PLL

4.1 Review

Many research groups worldwide have made significant progress in stabilizing the phase in long fiber interferometry. A notable example is the work done at the University of Colorado [21], where they successfully implemented a 38 km fiber between their laboratories. The results from this experiment are shown in fig.28, which presents the loss in decibels as a function of fiber length. These measurements are critical for understanding the attenuation characteristics in long-distance fiber-optic systems, especially when applied to interferometric setups.
Additionally, the group at the University of Colorado conducted phase noise measurements to evaluate the impact of fiber length on phase stability, as shown in fig.29. These results are crucial for assessing the ability to maintain phase coherence over long fiber paths, which is essential for high-precision interferometric measurements.

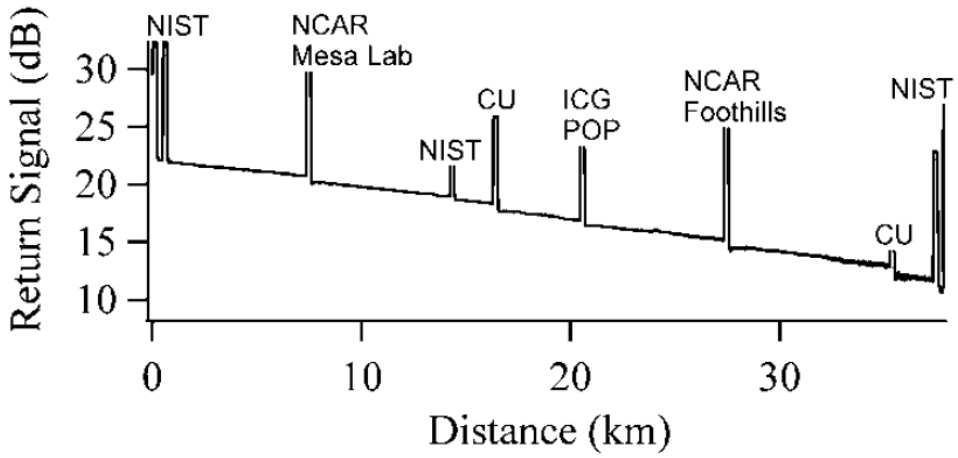

Figure 28: Decibel loss as a function of fiber length.
(Source: [21])

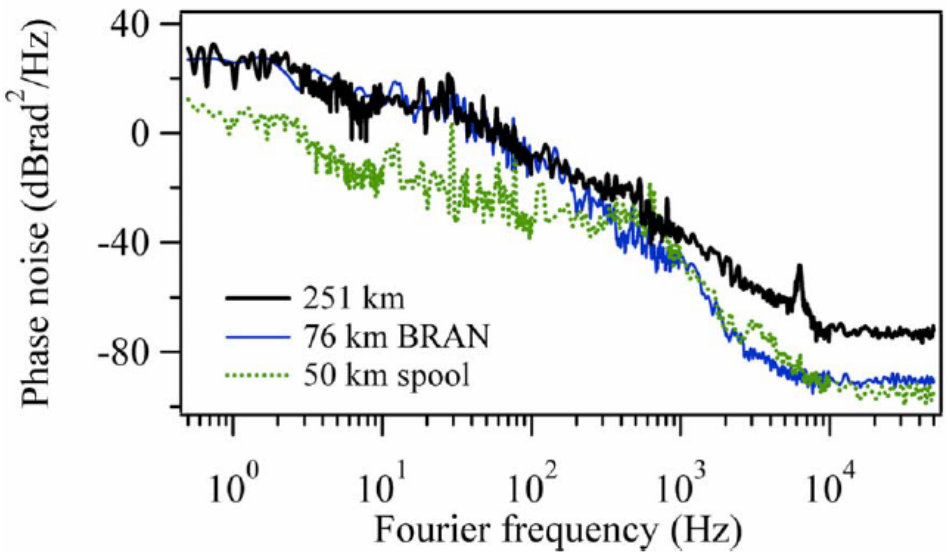

Figure 29: Phase noise measurements for long fiber interferometry.
(Source: [21])

Given that even longer fiber arms should be possible, the focus of this chapter is to replace the current fiber stretcher with two Acousto-Optic Modulators (AOMs) and upgrade the feedback system with a more advanced Phase-Lock Loop (PLL). This modification aims to stabilize the phase over significantly longer fiber lengths, potentially extending up to 100 km. The goal is to improve the interferometer's phase stability and enable long-distance interferometric measurements, laying the groundwork for further developments within the research group.

The proposed changes, including the integration of AOMs and PLLs, are designed to enhance the system's ability to compensate phase noise and achieve long-term phase coherence, even in the presence of significant environmental noise. These advancements are essential steps toward achieving the ultimate objective of maintaining stable phase over extended fiber paths.

4.2 AOM and PLL

AOM:

As previously mentioned, the fiber stretcher has been replaced by an acousto-optic Modulator (AOM) [33]. One key difference between the AOM and the fiber stretcher is that the AOM operates in a frequency-dependent manner, where the fiber stretcher was phase-dependent. The AOM shifts the frequency of one arm of the interferometer by 40 MHz. To ensure the accuracy of the phase stabilization, a copy of the AOM's drive signal is used to generate a DC error signal that is proportional to the phase difference. This phase error signal is then fed into the Voltage-Controlled Oscillator (VCO), which adjusts the AOM drive signal, effectively stabilizing the frequency (feedback mechanism). Additionally, it is essential to position the AOM as close as possible to the final beam splitter in the interferometer. This minimizes any additional length introduced by the fiber spool, which could affect the operation of the Phase-Lock Loop (PLL) by introducing unwanted delays or phase shifts.

The incorporation of two AOMs confers several notable advantages, particularly in the stabilization of the interferometric setup:

Enhanced phase stability: The deployment of two AOMs allows the precise fine-tuning of the phase of the quantum signals transmitted. This contributes to an improvement in the interference visibility.

Active noise cancellation: The second AOM facilitates the active cancellation of phase noise induced by fiber imperfections and environmental fluctuations. This mechanism effectively mitigates the impact of external disturbances, such as temperature variations or mechanical vibrations, that may introduce phase shifts in the optical fibers, ensuring real-time correction of such errors.

Simultaneous key streaming and channel stabilization: By utilizing two AOMs, one can be dedicated to stabilizing the fiber channels, while the other adjusts the phase of the incoming signals. This dual-functionality enables the concurrent processes of key streaming and phase stabilization, significantly enhancing the operational efficiency and robustness of the system.

Extended duty cycles: The precise control over the optical phase provided by two AOMs ensures long-term system stability, thereby enabling longer duty cycles. This, in turn, allows for a more efficient use of the available resources, improving the overall performance and practicality of the system for real-world applications.

PLL setup:

The core component of the new setup is the phase-lock loop (PLL), depicted in fig.30. The PLL serves a similar function as the feedback board in the previous setup but with a more sophisticated control mechanism. The output signal from the interferometer is fed back to the AOM, ensuring continuous phase stabilization. The PLL operates by comparing the phase of the output signal to the reference, adjusting the frequency of the AOM accordingly to keep the phase locked.

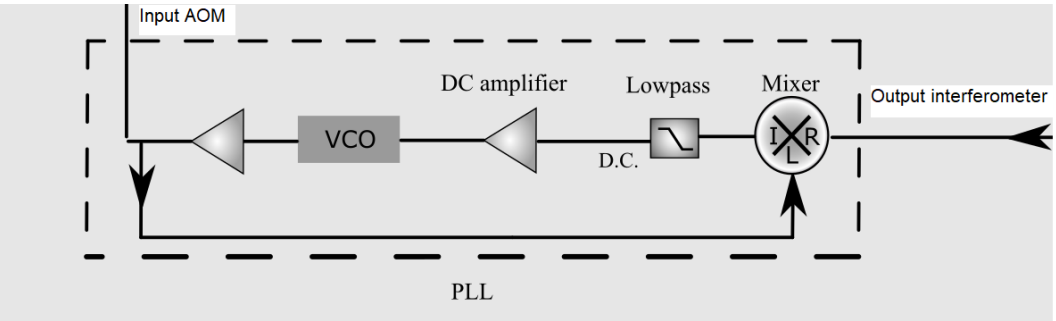

Figure 30: Schematic setup of the Phase-Lock Loop (PLL).

One of the primary considerations for the PLL's performance was ensuring that the DC power supply [38] provided sufficient power to all components of the loop while maintaining a stable DC output. This constant power supply is essential for the PLL's ability to function without fluctuations, ensuring precise control over the system.

Mixer:

The output signal from the interferometer is initially routed through a mixer [34] followed by a low-pass filter [35]. The purpose of the mixer is to combine the interferometer's signal with a copy of the AOM drive signal, producing a heterodyne beat note. The low-pass filter removes the high-frequency components, leaving behind a demodulated DC signal that corresponds to the phase difference between the interferometer arms. This DC signal is generally too weak for measurement, so it is amplified by an amplifier [36].

VCO:

After amplification, the signal is passed through a Voltage-Controlled Oscillator (VCO) [37]. The VCO produces an output frequency f that is linearly dependent on the incoming control voltage V. This linear relationship is crucial for precise frequency tuning and phase correction. The voltage-to-frequency dependency of the VCO is relatively linear over a wide range, ensuring stable and predictable phase adjustments.

The output from the VCO is then amplified again [36] to provide sufficient power for the AOM [33], which requires a significant amount of energy to operate effectively.

In fig.31, the linear behavior of the VCO used in this setup is shown, illustrating its predictable and stable response to the input voltage.

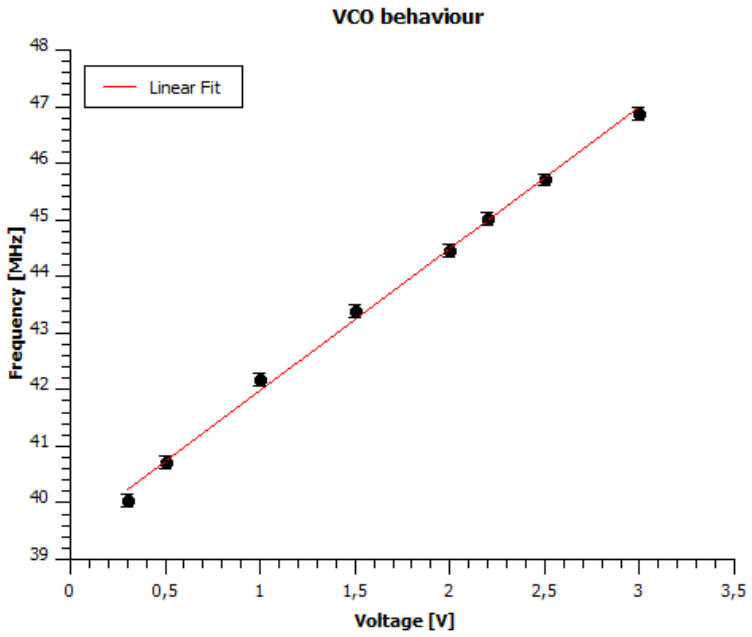

Figure 31: Voltage-to-frequency behavior of the Voltage-Controlled Oscillator (VCO) used in the PLL.

4.3 Implemantation and calculation

Long fiber Mach-Zehnder interferometry is also highly relevant in other fields, such as quantum key distribution (QKD), and there are numerous promising projects in this direction [17] [18].

Quantum key distribution (QKD) ensures secure communication by exploiting the principles of quantum mechanics, allowing two distant parties to share a cryptographic key. However, traditional QKD protocols suffer from severe limitations in long-distance communication due to exponential losses over fiber-optic links. The recently proposed twin-field quantum key distribution (TF-QKD) protocol has emerged as a promising solution to this issue, offering a fundamentally superior rate-loss scaling, making it suitable for long-distance secure communication. A major challenge in implementing TF-QKD is maintaining phase coherence between the lasers at Alice and Bobs stations, as phase instability due to environmental noise can lead to errors in the interference measurements at Charlie. Traditionally, this challenge was addressed by using a dedicated service fiber for phase synchronization. However, recent advancements have demonstrated the possibility of implementing TF-QKD without requiring such a service fiber. By employing ultrastable lasers and optical frequency combs for phase-locking, the new approach stabilizes the system over long distances without additional infrastructure. These improvements enable TF-QKD to operate effectively over hundreds of kilometers of fiber, achieving high key generation rates and maintaining security even in the presence of fiber loss and phase noise. This breakthrough paves the way for scalable, long-distance quantum communication networks, with TF-QKD potentially playing a crucial role in the future of secure telecommunications.

The paper of C. Clivati [17] demonstrates a real-world implementation of twin-field quantum key distribution (TF-QKD) over a 206 km deployed fiber network with 65 dB loss (fig.: 32). The authors utilize techniques adapted from frequency metrology to achieve real-time stabilization of phase fluctuations in the interferometer.

The key components include:

- Ultrastable lasers with ≈ 1 Hz linewidth used as reference sources.
- Sensing laser transmitted alongside the quantum signal using dense wavelength-division multiplexing (DWDM).
- Interferometric phase detection at the central node (Charlie) using beat notes between the sensing laser and a local oscillator.
- Analog feedback loop that dynamically adjusts an AOM to compensate for phase drift.

The approach enables simultaneous quantum key streaming and phase stabilization, reducing the quantum bit error rate (QBER) due to fiber noise to less than 1 %, and extending the coherence time by over three orders of magnitude compared to earlier implementations.

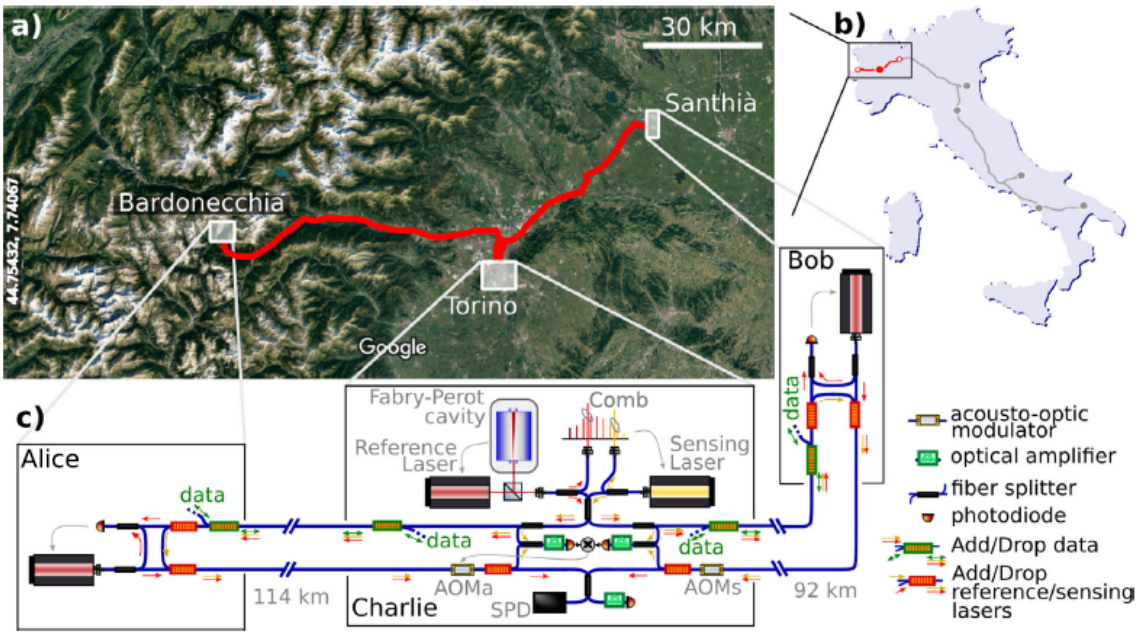

Figure 32: Coherent phase transfer for real-world twin-field quantum key distribution
(Source: [17])

In contrast to previous methods, Zhou et al. [18] remove the need for a service fiber by utilizing independently generated frequency combs at the sender nodes (Alice and Bob).

Key features include:

- Local generation of frequency combs using phase modulation of narrow-linewidth lasers.
- Selection of wwo wavelengths: one for quantum signals and another for phase reference.
- Photon-counting PID controller for real-time phase feedback based on single-photon detections at Charlie.
- Dual-wavelength stabilization: One comb line is used for stabilizing the channel phase, while another carries the quantum information.

This open-channel architecture supports asymmetric links up to 100 km difference, reaches distances of 615.6 km, and eliminates the need for closed interferometric configurations or shared optical clocks (fig.: 33). .

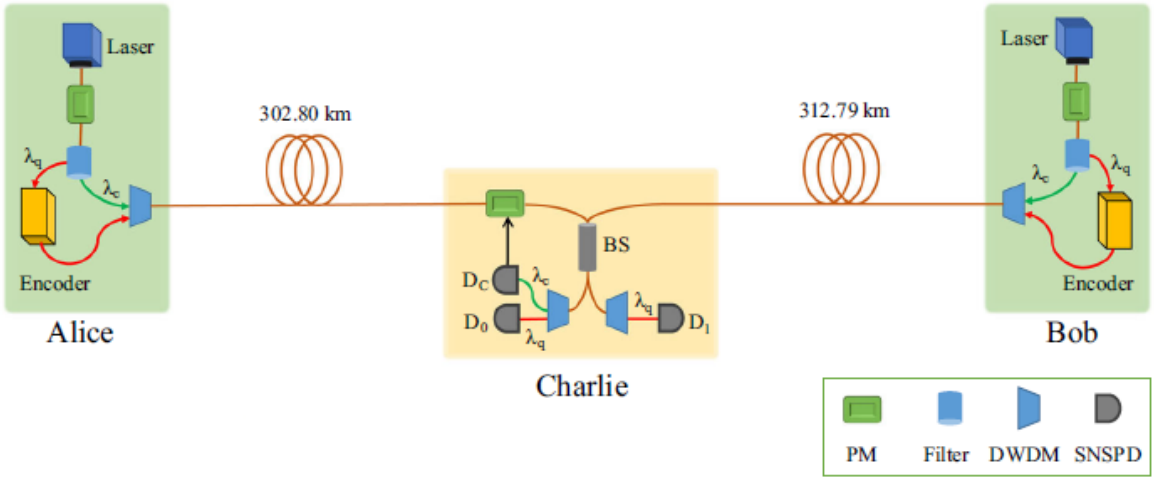

Figure 33: Twin-field quantum key distribution without optical frequency dissemination
(Source: [18])

In both papers, and in advanced interferometry in general, two AOMs are often employed with distinct but complementary functions:

AOM 1: Modulation and frequency shift

- Introduces a controlled frequency offset by 40 MHz
- Allows for heterodyne detection of phase shifts
- Can be placed in one interferometer arm for dynamic phase correction.

AOM 2: Isolation and interference control

- Can be used in the second arm or at the remote node.
- Ensures both arms experience symmetric frequency shifts
- Enables self-heterodyne detection when light returns from remote ends.

Together, two AOMs provide broadband control over the interferometer's relative phase, enabling compensation of environmental drifts while maintaining stable interference.

Calculation:

Based on the insights gained from the two referenced papers, one can now adopt a novel schematic approach for the fiber interferometer that also incorporates two AOM's as seen in fig.: 34.

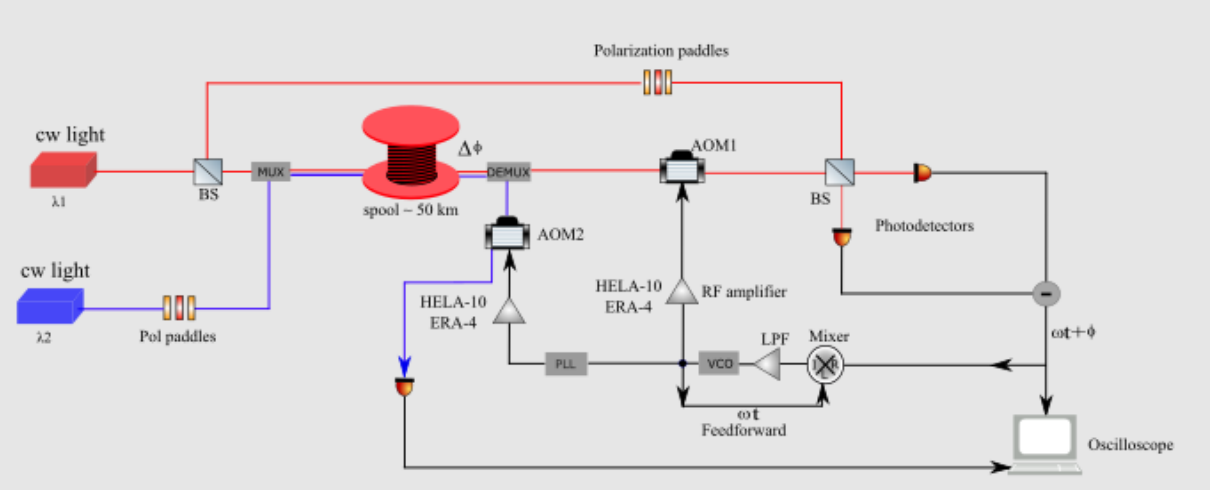

Figure 34: Approach for the new phase stabilization

An optical fiber-based Mach-Zehnder interferometer configuration is considered, comprising two independent cw laser sources operating at distinct optical frequencies, ν_A and ν_B, respectively. The electric field emitted from each laser is expressed as:

$$E_A(t) = E_0^A \cdot e^{i2\pi\nu_A t}, \qquad E_B(t) = E_0^B \cdot e^{i2\pi\nu_B t} \tag{16}$$

These fields are coupled into optical fibers of lengths L_A and L_B, with refractive indices n_A and n_B. During propagation, phase shifts are accumulated due to both the deterministic optical path and stochastic environmental perturbations, such as temperature fluctuations and mechanical stress. The resulting electric fields after propagation are given by:

$$E_A(t) = E_0^A \cdot e^{i(2\pi\nu_A t + \phi_A(t))}, \qquad E_B(t) = E_0^B \cdot e^{i(2\pi\nu_B t + \phi_B(t))} \tag{17}$$

with total phase contributions:

$$\phi_A(t) = \frac{2\pi n_A L_A}{\lambda_A} + \phi_A^{\text{noise}}(t), \qquad \phi_B(t) = \frac{2\pi n_B L_B}{\lambda_B} + \phi_B^{\text{noise}}(t) \tag{18}$$

To detect the relative phase between the two fields, each optical path includes an acousto-optic modulator (AOM), introducing frequency shifts f_A and f_B. The shifted frequencies become:

$$\nu'_A = \nu_A + f_A, \qquad \nu'_B = \nu_B + f_B \tag{19}$$

The corresponding electric fields after modulation are:

$$E''_A(t) = E_0^A \cdot e^{i(2\pi\nu'_A t + \phi_A(t))}, \qquad E''_B(t) = E_0^B \cdot e^{i(2\pi\nu'_B t + \phi_B(t))} \tag{20}$$

The output field is:

$$E_{\text{out}}(t) = \frac{1}{\sqrt{2}} \left(E''_A(t) + E''_B(t)\right) \tag{21}$$

The measured output intensity is proportional to the squared magnitude of the total electric field:

$$I(t) \propto |E_{\text{out}}(t)|^2 = \frac{1}{2} \left[(E_0^A)^2 + (E_0^B)^2 + 2E_0^A E_0^B \cos(2\pi\Delta\nu \cdot t + \Delta\phi(t))\right] \tag{22}$$

where $\Delta\nu = \nu'_A - \nu'_B = (\nu_A + f_A) - (\nu_B + f_B)$ is the effective frequency offset, and $\Delta\phi(t) = \phi_A(t) - \phi_B(t)$ is the relative optical phase.

To ensure phase coherence, a Phase-Locked Loop (PLL) is employed. The photo-detected beat signal is mixed with a reference oscillator and filtered to extract a baseband phase error. This error signal is used to control a voltage-controlled oscillator (VCO) driving one of the AOMs. This dynamic locking mechanism allows the interferometer to suppress environmental disturbances in real-time.

The integration of two AOMs with a feedback control loop offers two critical benefits. Firstly, the frequency offset introduced by the AOMs shifts the interference pattern to a heterodyne frequency, enhancing detection sensitivity and enabling phase demodulation. Secondly, dynamic tuning of one AOM in response to the feedback signal stabilizes the system against slow phase drifts, preserving coherence even between uncorrelated laser sources.

This configuration represents a foundational approach for fiber-based interferometric systems employed in quantum communication. Techniques utilizing two acousto-optic modulators (AOMs) in conjunction with a phase-locked loop (PLL) offer the potential for maintaining precise phase control over extended fiber links exceeding 100 km. Such methods have become standard practice in implementations like TF-QKD, where long-distance phase coherence is essential. The architecture presented here is expected to serve as a solid foundation for future scientific investigations within the research group.

5 Conclusion

In theory, an experimental setup to measure the phase shift in an interferometer due to the height difference of one arm should be achievable at a laboratory scale. However, constructing such an experimental setup involves numerous intermediate steps, each often accompanied by significant technical challenges. One of the primary difficulties encountered in this experiment was stabilizing the phase over long arm lengths, which is critical to making the interferometer sensitive enough to measure the desired phase shift.

The decision to use fiber interferometry instead of traditional free-space interferometry was a promising starting point, as it offered increased stability and reduced susceptibility to environmental noise. A first version of the interferometer setup was built, with initial configuration included a fiber stretcher and a feedback board. The feedback board, functioning primarily as a third-order low-pass filter, was instrumental in controlling unknown noise sources. This enabled the system to stabilize the phase, yielding a clean signal on the oscilloscope.

However, as longer fibers were integrated into the system, the performance degraded. The signal quality deteriorated, and the phase drifted out of lock more quickly. Even with a 15 m fiber, the system reached its performance limit. Attempts to mitigate the noise by shielding one of the arms of the interferometer did not significantly improve the situation, highlighting the inherent limitations of the original setup.

To overcome these challenges, a second iteration of the experimental setup was required. The first major modification was the replacement of the fiber stretcher with two Acousto-Optic Modulators (AOMs). AOMs are known to have better phase-stabilizing properties compared to fiber stretchers, leading to immediate improvements in phase control. The second key improvement was the upgrade of the feedback loop by introducing a Phase-Lock Loop (PLL). The PLL offers more precise and efficient phase stabilization, significantly enhancing the systems ability to maintain phase coherence over longer fiber lengths.

The integration of two AOMs and a PLL is expected to significantly enhance phase stability in fiber-based interferometers, particularly when operating with extended arm lengths. Compared to previous approaches relying on fiber stretchers, this technique should offer advantages in terms of responsiveness, stability, and scalability. Experimental evidence from twin-field quantum key distribution (TF-QKD) demonstrates that such configurations can support interferometric coherence over distances well beyond 100 km. With this outlook, the present work aims to provide a solid foundation for future experimental developments within the research group.

6 Bibliography

References

6.1 List of references

[1] A. Khrennikov, The present situation in quantum theory and its merging with general relativity, *Foundation of Physics*, 47, 1077/1099, 2017

[2] https://www.spektrum.de/thema/albert-einstein-und-die-relativitaetstheorie/1346052

[3] https://www.nobelprize.org/prizes/physics/2022/zeilinger/facts/

[4] R.W.Peterson, C.Hilweg, R. Silvestri and P. Walther, Optical fiber noise cancellation for fundamental tests of gravity and quantum mechanics

[5] https://turis.univie.ac.at/research/gravites/

[6] M.Pössel, The Shapiro time delay and the equivalence principle, *arXiv:2001.00229v1*, 2019

[7] https://www.nature.com/articles/d41586-023-01938-6

[8] J. Bedford, An introduction to string theory, *arXiv:1107.3967v3*, 2012

[9] M. Arndt, M. Nairz, O. Vos-Andreae, Wave-particle duality of C_{60} molecules, *Nature*, Vol. 401, 680-682, 1999

[10] https://www.cs.princeton.edu/courses/archive/fall06/cos576/papers/zetie_et_al_mach_zehnder00.pdf

[11] https://www.nobelprize.org/prizes/physics/2017/press-release/

[12] https://physicswave.com/michelson-interferometer-construction-and-working/

[13] Clay K. Kirkendall and Anthony Dandridge, Overview of high performance fibre-optic sensing, *Journal of physics*, 37 (2004), R197-R216, PII: S0022-3727(04)39793-7

[14] https://www.rp-photonics.com/polarization_of_light.html

[15] https://www.electronics-tutorials.ws/systems/feedback-systems.html

[16] R. Simon and N.Mukunda, Minimal three-component SU(2) gadget for polarization optics, *Science direct*, Vol. 143, number 4 and 5, January 1990

[17] Cecilia Clivati, Alice Meda , Simone Donadello , Salvatore Virzì , Marco Genovese, Filippo Levi1, Alberto Mura , Mirko Pittaluga, Zhiliang Yuan, Andrew J. Shields, Marco Lucamarini, Ivo Pietro Degiovanni, Davide Calonico1, Coherent phase transfer for real-world twin-field quantum key distribution, *nature communications*, (2022), 13:157

[18] Lai Zhou, Jinping Lin, Yumang Jing, Zhiliang Yuan, Twin-field quantum key distribution without optical frequency dissemination, *nature communications*, (2023), 14:928

[19] P. Horowitz and W. Hill, Art of electronics, *Cambridge University Press*, third edition. 2015

[20] Thomas G. Giallorenzi, Joseph A. Bucaro, Anthony Dandridge, G. H. Sigel, JR., James H. Cole, Scott C. Rashleigh, Member, IEEE, Richard G. Priest, Optical Fiber Sensor Technology, *IEEE Transactions on microwave theory and techniques*, Vol. MTT-30, NO. 4, April 1982

[21] P.A. Williams, W.C. Swann and N.R. Newbury, High-stability transfer of an optical frequency over long fiber optics, *J. Opt: Soc. Am. B*, Vol.25, No.8, August 2008

6.2 List of components

[22] Link to the homepage of the used laser: https://punchout.thorlabs.com/thorproduct.cfm?partnumber=ORS-DL
Or PDF download link: https://punchout.thorlabs.com/drawings/9b8ebfc076f4abe-EF4F28D9-BFAF-CBC7-CC5D967FEB058D11/ORS-DL-SpecSheet.pdf

[23] Link to the used fibers: https://www.thorlabs.com/newgrouppage9.cfm?objectgroup_id=9152

[24] Download link for the used fiber stretcher: https://www.optiphase2.com/wp-content/uploads/2024/07/PZ1-Data-Sheet-Rev-H2-PI.pdf

[25] Download Link for the used function generator: https://docs.rs-online.com/9c12/A700000010216918.pdf

[26] Link for the used polarization stage/paddles: https://www.thorlabs.com/NewGroupPage9_PF.cfm?ObjectGroup_ID=343

[27] Link to the homepage of the used photo detector with amplifier: https://www.femto.de/en/silizium-und-ingaas-fotoempfaenger-fotodetektoren/dc-bis-200-mhz-variable-verstaerkung-oe-300/
Or PDF download link: https://www.femto.de/images/pdf-dokumente/de-oe-300-in-01.pdf

[28] Link to the homepage of the used oscilloskop: https://www.tek.com/en/datasheet/digital-storage-oscilloscope-tbs2000b-series-datasheet
Or PDF download link: file:///C:/Users/Lukas/Downloads/TBS2000B-Datasheet_3GW615096.pdf

[29] Link to the homepage of the used powermeter: https://www.thorlabs.us/thorProduct.cfm?partNumber=PM100D
Or PDF download link: https://www.thorlabs.us/drawings/dfe6ea19849f35c6-F2BE18B1-A452-0175-81BFAD974F497242/PM100D-AutoCADPDF.pdf

[30] Link to the homepage of the used power supply with fan: https://www.digikey.at/en/product-highlight/q/qualtek/power-and-cooling?utm_adgroup=Power%20Supply&utm_source=bing&utm_medium=cpc&utm_campaign=Dynamic%20Search_EN_Product&utm_term=power%20supplies&productid=&utm_content=Power%20Supply&utm_id=bi_cmp-420488685_adg-1306220177401610_ad-81638835947985_dat-2333438552187382:loc-10_dev-c_ext-_prd-&msclkid=6c20d57fef7e1034e8eeb3ba487018ff
Or PDF download link fan: https://www.qualtekusa.com/images/Fans/pdf_files/FAA1-08025.pdf

[31] Link to the homepage of the used PCB board: https://www.digikey.at/de/products/detail/sparkfun-electronics/PRT-12002/17828026?utm_adgroup=&utm_source=bing&utm_medium=cpc&utm_campaign=PMax%20Shopping_Product_High%20ROAS&utm_term=&productid=17828026&utm_content=&utm_id=bi_cmp-627379374_adg-1305121451303609_ad-81570146302228_pla-2333369832852624_dev-c_ext-_prd-17828026&msclkid=f581bff26ba417ca5ffad937c5a4edc5
Or PDF download link: https://cdn.sparkfun.com/datasheets/Prototyping/breadboard.pdf

[32] Link for the used spool: https://www.itu.int/ITU-T/recommendations/rec.aspx?rec=13076#:~:text=Recommendation%20ITU-T%20G.652%20describes%20the%20geometrical%2C%20mechanical%20and,also%20be%20used%20in%20the%201550%20nm%20region.

[33] Link to the homepage of the used AOM: https://www.brimrose.com/fiber-coupled-ao/fiber-coupled-acousto-optic-modulators
Or PDF download link: https://static1.squarespace.com/static/58cd62b759cc688ab46997dd/t/64aed6f87456cb63a5eba82c/1689179897084/FCAOM.pdf

[34] Download link for the used mixer https://www.minicircuits.com/pdfs/ZAD-2.pdf

[35] Link to the homepage of the used lowpass filter: https://www.thorlabs.com/newgrouppage9.cfm?objectgroup_id=8613
Or PDF download link: https://www.thorlabs.com/drawings/dc5770428a5e8ee-217FEAE0-B522-ED9B-F25564FBB624B221/EF506-AutoCADPDF.pdf

[36] Link to the homepage of the used amplifier: https://www.minicircuits.com/

WebStore/dashboard.html?model=HELA-10%2B
Or PDF download link: https://www.minicircuits.com/pdfs/HELA-10+.pdf

[37] Link to the homepage of the used VCO: https://www.minicircuits.com/WebStore/dashboard.html?model=ZX95-43-S%2B
Or PDF download link: https://www.minicircuits.com/pdfs/ZX95-43-S+.pdf

[38] Download Link for the used DC power supply: https://docs.rs-online.com/17e6/0900766b81409df0.pdf